2011

Predictability of Dry Season Reforecasts over the Tropical South American Region

Adam J. Frumkin

THE FLORIDA STATE UNIVERSITY

COLLEGE OF ARTS AND SCIENCES

PREDICTABILITY OF DRY SEASON REFORECASTS OVER THE TROPICAL SOUTH AMERICAN REGION

By

ADAM J. FRUMKIN

A thesis submitted to the
Department of Earth Ocean and Atmospheric Sciences
in partial fulfillment of the
requirements for the degree of
Masters of Science

Degree Awarded:
Spring Semester, 2011

The members of the committee approve the thesis of Adam Joseph Frumkin defended on March 17th 2011.

_____
Vasubandhu Misra
Professor Directing Thesis

_____
Henry Fuelberg
Committee Member

_____
Philip Sura
Committee Member

The Graduate School has verified and approved the above-named committee

This thesis is dedicated to my friends and family. Without them my education and this work would not have been possible

ACKNOWLEDGEMENTS

I would like to acknowledge Dr. Vasu Misra who encouraged me to conduct this research and offered much guidance along the way. I would also like to thank Dr. Henry Fuelberg, who I believe was influential in my acceptance to FSU, and Dr. Philip Sura who served on my committee. I also need to thank Dr. Steven Chan who was beyond helpful throughout this process. My family has always been there for me and for that I am grateful. Lastly, without my friends at FSU and the members of Dr. Misra's lab this process would have been far less seamless and for that I am forever indebted to them.

TABLE OF CONTENTS

LIST OF TABLES

LIST OF FIGURES

LIST OF ACRONYMS

AN	Anomaly Nesting
ARB	Amazon River Basin region
AUC	Area Under the ROC curve
AWP	Atlantic Warm Pool
CAMS	Climate Assessment and Monitoring System
CFS	NCEP Climate Forecast System
CFSR	NCEP Climate Forecast System Reanalysis
CLLJ	Caribbean low-level jet
CMAP	CPC Merged Analysis of Precipitation
CPC	NCEP Climate Prediction Center
CRU	Climate Research Unit
DJF	December–January–February
GCM	global climate model
GODAS	Global Ocean Data Assimilation System
GPCC	Global Precipitation Climatology Centre
GPLLJ	Great Plains low-level jet
ITCZ	Intertropical Convergence Zone
JJA	June–July–August
LA	leaf area
LAI	leaf area index
MRF	NCEP Medium Range Forecast PBL scheme
NCEP	National Centers for Environmental Prediction
NOAH	NCEP-Ohio State-US Air Force-NWS Hydrology Laboratory
PBL	planetary boundary layer
RCM	regional climate model
ROC	Relative Operative Characteristic curve
RSM	Regional Spectral Model
RSM-AN	Regional Spectral Model with Anomaly Nesting
SA	South America
SALLJ	South American low-level jet
SAM	South American monsoon
SAS	Simplified 1 Arakawa-Schubert cumulus convection scheme
SASH	South Atlantic subtropical high
SLP	sea level pressure
SMO	Sierra Madre Occidental range
SSBC	Scale Selective Bias Correction
ST	Subtropical region
TRMM	Tropical Rainfall Measuring Mission

ABSTRACT

Atmospheric conditions during the dry season of the South American monsoon are instrumental in the initiation of convection during the wet season and are strongly correlated to SSTs within the Atlantic Warm Pool. Subsequently, accurate seasonal prediction of temperature and rainfall during the dry season has the potential to improve our understanding of and the predictability of these variables during future seasons.

In this study, we review the fidelity of South American dry season (June-July-August) reforecasts from one global climate model (GCM), and one downscaled regional climate model (RCM). Additionally, we evaluate a second integration of the RCM that uses a bias correction method called anomaly nesting, which is designed to remove the bias of the GCM before the downscaling process is performed. The models are integrated for seven dry seasons (2001–2007), and each season consists of six ensemble members. For this study, we focus on two primary regions: the Amazon River Basin (ARB) and the subtropical region (ST).

There are three objectives of this research. The first is to locate regions of model bias for two-meter air temperature and for precipitation within the ARB and the ST using NCEP Climate Forecast System Reanalysis (CFSR) as a comparison dataset. The second is to evaluate the predictability of above normal, normal, and below normal occurrences of the two variables using potential predictability ratios and calculations of the area under the relative operative characteristic (ROC) curve (AUC). Through this analysis we should be able to determine whether downscaling or anomaly nesting improve upon the skill of the GCM. Lastly we wish to evaluate how the three models depict land-atmosphere interactions during the dry season and compare their results with results from CFSR.

The models produced the largest biases of both variables over elevated terrain and within the Intertropical Convergence Zone (ITCZ). However, neither of these locations significantly impacts the ARB or the ST. Signal-to-noise ratios show that the ARB exhibits more potential predictability than the ST and that temperature exhibits more potential predictability than precipitation. AUCs confirm that temperature is more skillfully predicted than precipitation and that the models exhibit more skill in the ARB than in the ST. AUCs show that the downscaled and the downscaled with anomaly nesting integrations display more skill than the GCM

integration, particularly in the ARB. Lastly, we find conflicting results between the models and CFSR regarding how the land and the atmosphere interact during the dry season. However, a full moisture budget analysis is needed to completely resolve land-atmosphere feedbacks and that is beyond the scope of this study.

CHAPTER ONE

INTRODUCTION

Seasonal climate prediction using global climate models (GCMs) is a growing trend in the fields of climate and atmospheric science. In the past, GCMs were limited to use within regions that exhibited teleconnections to global scale atmospheric phenomena because of their coarse resolution. Recently, seasonal climate prediction using higher-resolution regional climate models (RCMs) has been occurring with increasing regularity. Regional forecasts are frequently generated by dynamically or statistically downscaling the output generated by a GCM to finer resolutions using high-resolution RCMs. The downscaling model (i.e., the RCM) should, in theory, provide a more accurate representation of the finer scale physics, dynamics, and topography than the GCM does and thus provide a more skillful forecast.

This study investigates the implications of downscaling the National Centers for Environmental Prediction (NCEP) coupled Climate Forecast System (CFS) over South America (SA), using the NCEP-Scripps Regional Spectral Model (RSM). In this study, we also evaluate the effect of applying a bias correction process to the GCM before the downscaling is performed with the RCM. The bias correcting process used in this study is referred to as anomaly nesting. Hereafter, the RSM integration with the anomaly nested bias correction is referred to as RSM-AN. In this study, we focus on verifying the reforecasts produced for June, July, and August (2001–2007) by three models (CFS, RSM, and RSM-AN). These data represent seven years of the South American monsoon (SAM) dry season.

1.1 South American Climatology and the South American Monsoon

The SAM has been studied little compared to other monsoons around the world but is arguably the most important feature of the South American climate. In fact, it was not until Zhou and Lau (1998) analyzed the South American climate that SA was acknowledged as having a monsoon climate. Despite this, some scholars still debate whether or not South America's monsoon meets the "classic" (e.g., East Asian monsoon) definition of the word. Generally, a monsoon climate exhibits a distinct seasonal cycle in temperature and precipitation and seasonal reversal of lower tropospheric winds. Over SA, there is not an obvious reversal of the winds

because of the annual persistence of easterlies in the tropics. However, it is possible to produce a reversal in the winds when the annual mean is removed (Figure 1.1). Perhaps it is most accurate to state that the SAM is modulated by seasonal fluctuations of the persistent trade winds, rather than a seasonal reversal in the wind field.

Although the SAM lacks a seasonal wind reversal, it does exhibit many of the other characteristics that define a classic monsoon. For example, indisputable evidence exists of a well defined annual cycle in precipitation. A wet phase occurs during austral summer [December–February (DJF)] and a dry phase occurs during the winter [June–August (JJA)]. There is a rapid increase in precipitation during the spring [September–November (SON)] and a decrease during March–May (MAM) (Figure 1.2; Raia, 2008). Additionally, the SAM exhibits the following: a large-scale land-sea temperature difference, a large-scale thermally direct circulation with a continental rising branch and an oceanic sinking branch, land-atmosphere interactions associated with elevated terrain and land surface conditions, surface low pressure and upper level anticyclone, and intense low-level inflow of moisture to the continent (Vera et al. 2006). The SAM is unique in that much of the affected land mass is located in the tropics as opposed to the subtropics, which results in less distinct seasonal temperature fluctuations.

Using a method developed for the Indian monsoon by Fasullo and Webster (2003), Raia (2008) identified the onset of the SAM for the majority of the monsoon region to be in mid-to-late October and the demise to be in late March. The onset in the northwest regions of the continent occurs in mid-to-late August and moves toward the southwest over time (Vera et al. 2006). The onset period is accompanied by a weakening and an eastward displacement of the South Atlantic subtropical high. As a result, the wind field over extreme southwestern Amazonia shifts from northerlies to northwesterlies, and over eastern Brazil the winds shift from easterlies to northeasterlies. These changes allow for enhanced moisture transport from Amazonia and the South Atlantic Ocean into the monsoon region (i.e., central SA).

Moisture transport into parts of the monsoon region is further enhanced by the South American low-level jet (SALLJ), which flows southward along the eastward facing slopes of the Andes Mountains. The main depository for moisture flux associated with the SALLJ is the La Plata River Basin, a large area in central SA that encompasses parts of five countries (Argentina, Bolivia, Brazil, Paraguay, and Uruguay). The SALLJ is observed nearly all year long and exists without synoptic scale forcing because of the interaction between the continental mean westerly

flow and the Andes Mountains and because of enhanced heating over the Andes. However, synoptic scale changes modulate the strength of the jet, which, in turn, modulates precipitation intensity in central SA (Liebmann et al., 2004).

The driving force behind the onset of the monsoon, and also the SALLJ, is enhanced heating in the elevated terrain of the Andes Mountains facilitated by the poleward migration of the sun. During the peak of austral summer (January), a major center of diabatic heating moves over the subtropical highlands (about 20°S), forcing the development of a heat low over Gran Chaco (Chaco low). This also results in a strong thermal gradient between the subtropical highlands and the surrounding oceans, forcing a shift in the wind regime to northwesterly and a maturation of the monsoon (Zhou and Lau, 1998). Additionally, low pressure systems propagating from east to west during the dry season occasionally contain precipitation, which increases the soil moisture and latent heat flux and decreases the sea level pressure (SLP; Raia, 2008). These conditions (increased diabatic heating and low level moisture) destabilize the atmosphere and facilitate onset of the wet season. The demise period exhibits an increase in SLP over the continent, an easterly moisture flux toward the Amazon region, a reduction in the northerly flow east of the Andes, and a reduction in vertical motions. These features primarily result from the westward shift of the South Atlantic subtropical high (SASH), which is facilitated by the equatorward shift of the sun. As the sun shifts poleward, heating over the elevated terrain weakens, the Chaco low weakens, the thermal gradient between the land and the ocean is reduced, and the SASH shifts to the west (Zhou and Lau, 1998). Raia (2008) noted that during JJA, when many regions of SA experience a minimum in precipitation, there is southeasterly moisture transport over Northeast Brazil driven by the subtropical high. Additionally, there is intense westward moisture transport over the Amazon region, which, because it lacks a southerly component, reduces the moisture transport to regions that typically experience the monsoonal cycle of rainfall.

1.2 Motivation

Although the SAM has only recently been acknowledged and the dry phase of the monsoon has received less attention than the wet phase, emerging research suggests that the dry phase may play a significant role in modulating the climate of SA and surrounding regions.

One source of motivation for this research is the important role that conditions in the Amazon rainforest during the dry season may play in initiating the wet phase of the SAM. Myneni et al. (2007) showed that changes in leaf area (LA) within the Amazon rainforest are strongly correlated with the seasonal cycle of precipitation and solar radiation. Unlike many other types of forests, which see an increase in LA during the wet season, the Amazon rainforest experiences a 25% increase in leaf area index (LAI) (relative to the wet season) over 60% of its area during the dry season. This increase in LAI is primarily driven by the increased amount of incoming solar radiation that accompanies the decrease in cloud-cover during the transition from the wet to the dry season. The authors suggested that the increase in leaf area during the dry season eventually leads to the initiation of the wet season; as leaf area increases, the amount of evapotranspiration and low-level moisture also increases. Increasing the amount of low-level moisture destabilizes the atmosphere and increases the probability of convection occurring toward the end of the dry season. Evidence of this forcing was observed in the 1980s, when many of the years with delayed wet season onset, had experienced slow increases in evapotranspiration at the end of the dry season. Because leaf area, and thus evapotranspiration, is modulated by agents other than the intensity of incoming solar radiation, such as water stress, being able to accurately forecast precipitation and temperature during the dry season may be beneficial. For example, by accurately forecasting precipitation during the dry season, we can estimate water stress and provide insight into the timing of the onset of the following wet season.

A second source of motivation for studying the dry phase of the SAM comes from the relationship it may have with the size and intensity of the Atlantic Warm Pool (AWP). The AWP plays a significant role in controlling the occurrence and intensity of Northern Hemisphere phenomena such as Atlantic hurricanes, the Great Plains low-level jet (GPLLJ), and the Caribbean low-level jet (CLLJ). An anomalously large (small) AWP weakens (strengthens) the GPLLJ, weakens (strengthens) the CLLJ, and reduces (increases) the tropospheric wind shear in the maximum development region of Atlantic hurricanes, thereby increasing (decreasing) the likelihood of cyclone development (Wang et al. 2008). Correlations between dry season rainfall and the following wet season rainfall show a strong positive relationship (correlation coefficients greater than 0.5) between the two variables, particularly within the box over northeast Brazil (Figure 1.3). Correlation coefficients also indicate a negative relationship between wet season rainfall within the box positioned over northeast Brazil in Figure 1.3 and SSTs within the region

of the AWP (Figure 1.4). This relationship implies that above (below) normal rainfall during JJA is followed by above (below) normal rainfall during the following DJF, which is followed by below (above) normal SSTs in the AWP region during the following JJA.

The primary motivation for this research is the analysis of the North American monsoon conducted by Chan and Misra (2009) in which they used the same three models that are used in this study. One motivating factor for their study, which also applies to the current research, is the results of Misra and Kanamitsu (2004). Misra and Kanamitsu (2004) showed success in seasonal prediction of the SAM using an anomaly nested RCM even when the GCM that was used to force the RCM was strongly biased. Chan and Misra (2009) found the major benefit of downscaling and anomaly nesting (AN) to be an improvement to certain dynamical fields such as winds, particularly those within low-level jets. This improvement can be at least partially attributed to the higher resolution of the RCM. They found that in topographically complex regions, such as the Gulf of California and the Sierra Madre Occidental (SMO) range the, CFS cannot be expected to accurately resolve small scale features. In fact, the CFS resolves the Gulf of California as a "block" protruding from the mainland, which results in an erroneous representation of SSTs in that region. The SMO exhibits a much more gradual slope in the CFS than it does in the RSM and also reaches a lower height. This causes higher than observed land surface temperatures in the CFS and can result in a poor representation of the climatological wind field. The downscaling process in the current study will improve the topography of the Andes Mountains which should also improve the representation of the SALLJ. Additionally, it is expected that more accurate representation of topography and coastlines will result in more accurate land surface temperatures in the downscaled RCM.

The goal of this research is to investigate the fidelity of SAM dry season reforecasts from the CFS and the RSM and to investigate the potential for using the downscaled runs for routine operational seasonal prediction. Previous studies have shown that downscaling with RCMs provides more accurate results due to their higher resolution. However, the benefit of higher resolution can be offset by the errors accrued from ingesting the biases of the GCM into the RCM during the downscaling process. Additionally, we review the anomaly nesting process which can remove some of the GCM bias from the RCM and further increase the accuracy of the forecast. As previously mentioned, this study investigates SAM dry season (JJA) reforecasts for SA using six-ensemble-member integrations of the CFS, RSM and AN-RSM. Chapter 2

describes the data and methods used to investigate the fidelity of the reforecasts, and the implications of using the downscaling and anomaly nesting processes. In Chapter 3 we discuss the skill of the models and suggest that faulty land-atmosphere feedbacks could be the cause of imperfect model forecasts. In Chapter 4 we summarize our results, provide conclusions, and suggest ideas for future work.

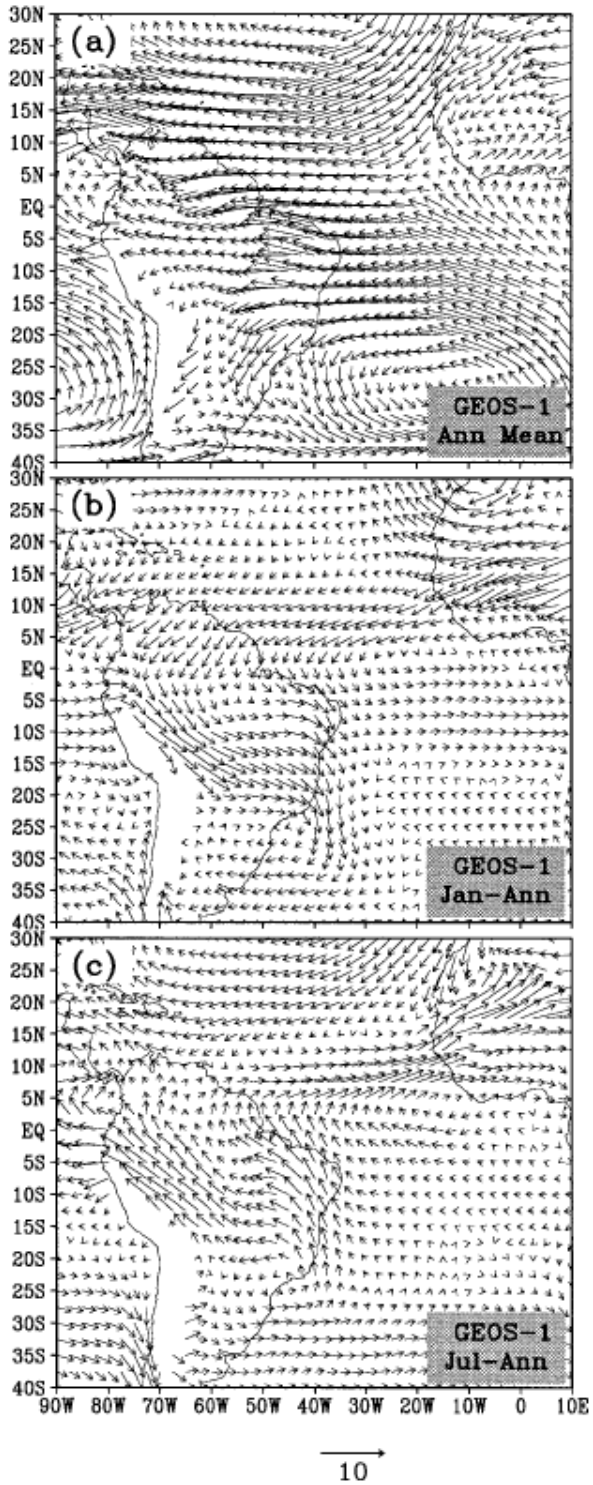

Figure 1. 1 From Zhou and Lau (1998) 900-hPa wind (m/s) for (a) annual mean, (b) January mean minus the annual mean, and (c) July mean minus annual mean.

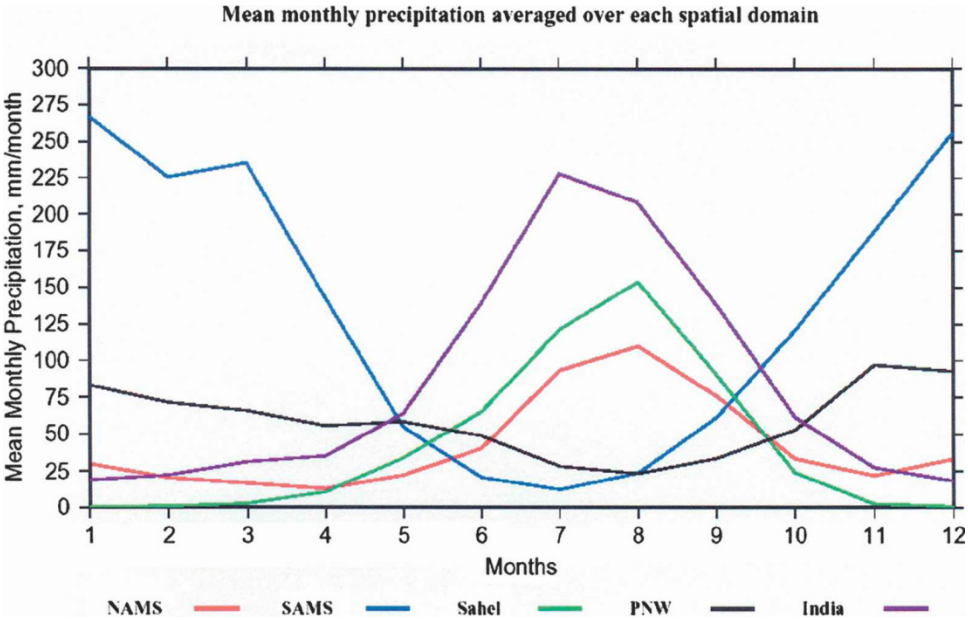

Figure 1. 2 From Raia (2008) Mean monthly precipitation (mm/month) is plotted for each month of the year. Different colored lines represent the annual cycle of precipitation for several of the most prominent monsoons across the globe. The South American monsoon is represented by the blue line labeled SAMS. A distinct minimum in precipitation can be seen during austral winter (JJA) and a maximum can be seen during austral summer (DJF).

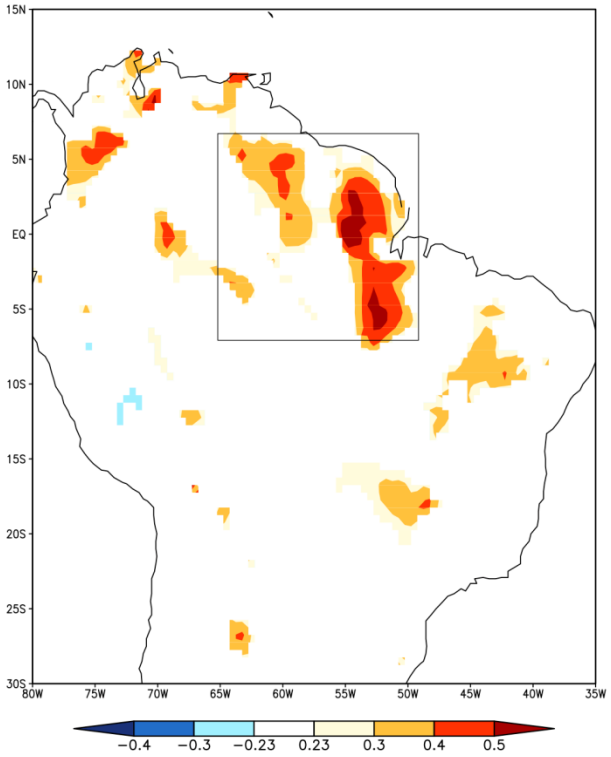

Figure 1. 3 Correlation of JJA rainfall with the following DJF rainfall. Only statistically significant values are shaded. The box represents the middle-lower reaches of the Amazon River. The boxed region is referenced in Figure 1.4.

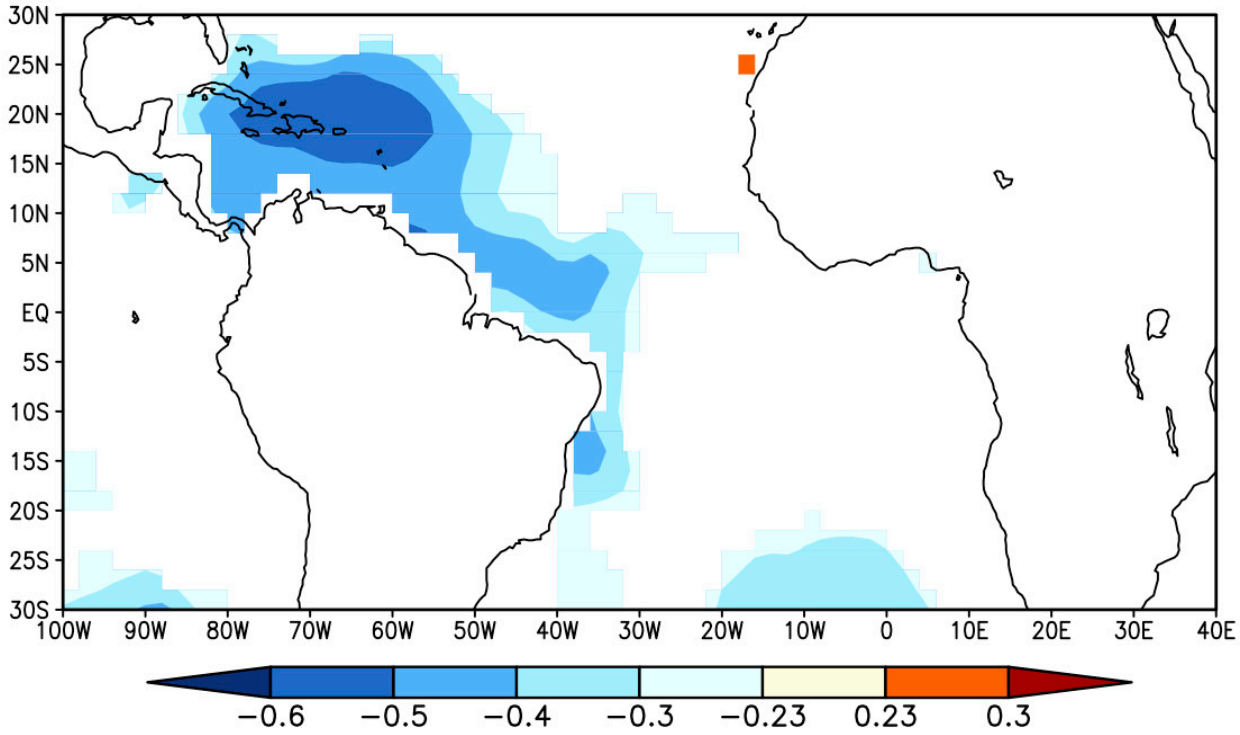

Figure 1. 4 Correlation of JJA ERSSTv3 with DJF Climate Research Unit (CRU) Rainfall averaged over the box in Figure 1.3. Only statistically significant values are plotted.

CHAPTER TWO

DATA AND METHODS

The model data used in this study are identical to those used by Chan and Misra (2009). Initial reforecasts are performed using the NCEP CFS. One downscaled reforecast is performed with the RSM using unmodified CFS data. A second downscaled run of the RSM is carried out after applying the anomaly nesting bias correction process to the CFS data. Model output is available at six hourly intervals.

2.1 Model Data

The three model integrations are conducted for June-September, 2001-2007. Model integrations are started at 0000Z 23 May 2001. Only data corresponding to the South American dry season (June, July, and August) are used in this study.

2.1.1 NOAA-NCEP CFS

The CFS is a fully coupled land-ocean-atmosphere dynamical seasonal weather prediction model. At the time of its release, the CFS provided a significant improvement over previous dynamical models. It also represented the first time in the history of the United States that a dynamical model was capable of achieving a level of skill (for temperature and precipitation predictions) that was comparable to the skill of statistical models used at the NCEP Climate Prediction Center (CPC; Saha et al. 2006).

The version of the CFS used in this study has 64 vertical sigma levels and is run at a triangular spectral truncation of T62 (~200-km Gaussian grid). It uses the Simplified 1 Arakawa-Schubert cumulus convection (SAS; Hong and Pan 1998), the NCEP Medium Range Forecast (MRF) planetary boundary layer (PBL) scheme (Hong and Pan 1996), and the Oregon State University land surface scheme (Mahrt and Pan 1987).

The CFS uses six ensemble members, each integrated for JJAS 2001-2007. This provides a total of forty-two simulations (six ensembles for each of the seven seasons). The ensemble members are generated by slightly perturbing the initial state of the atmosphere, accomplished by resetting the initial date of the atmospheric restart file after integrating the CFS for one week. This process is carried out six times to achieve the desired number of ensemble members. The

initial atmospheric conditions are acquired from the NCEP NCAR Reanalysis. Ocean initial conditions are obtained from the Global Ocean Data Assimilation System (GODAS; Behringer and Xue 2004). The initial land surface conditions are from the NCEP-DOE Reanalysis II (Kanamitsu et al. 2002). The initial ocean and land states are unchanged between ensemble members.

Additionally, we use separate CFS output that is identical to the output described in Saha et al. (2006). This version of the CFS has 15 ensemble members and was integrated from 1981-2003 (23 years). The CFS was initiated at the beginning of each calendar month and integrated for nine months. Each of the 15 ensemble members generated each month is initiated with different initial conditions acquired from 15 days in each month. A full description of how the days were chosen can be found in Saha et al. (2006). In this study we only use the JJA output from the integration that was initiated in June of each calendar year. This data is used to conduct a sensitivity experiment, the purpose of which is to determine whether we are underestimating or overestimating the potential skill of the CFS by limiting the number of years in our dataset to seven and by using only six ensemble members.

2.1.2 NCEP Scripps RSM

The NCEP-Scripps RSM, introduced in 1994, was initially designed to run with a high-resolution regional spectral model nested inside a coarse-resolution global spectral model of identical vertical levels (so as to avoid vertical interpolation) and identical model physics. At the time of its release, the RSM used a perturbation method of nesting. Juang and Kanamitsu (1994) also determined that nesting periods of three to six hours produced less noise than periods of one hour and that blending at the boundaries was not necessary.

Since its release, numerous changes have been made to the RSM. The most pertinent to this study are the updates to the model physics, including scale selective bias correction (SSBC; Kanamaru and Kanamitsu 2007). SSBC reduces the drift in the RCM and eliminates the need for multiple nesting to downscale from a coarse grid to a very fine grid (Chan and Misra 2009).

The RSM used in this study has 28 pressure sigma vertical levels and a 60-km horizontal resolution. This RSM has a lower resolution than is normally used because the model was run over a very large domain. The RSM was integrated over a significant portion of the North American and South American continents so that both the North American monsoon wet season and the South American monsoon dry season could by analyzed. The RSM uses the same

cumulus (SAS) and PBL (MRF) parameterizations that are used in the CFS. It also uses a different land surface scheme, the NCEP-Ohio State-US Air Force-NWS Hydrology Laboratory (NOAH) land scheme (Ek et al. 2003).

There are two RSM simulations used in this study. Both sets of integrations are run over the same time period as the CFS integration. The first integration, referred to as the RSM, is directly downscaled from the CFS and uses SSTs prescribed from the individual CFS ensemble integrations. The second integration, referred to as the RSM-AN, downscales after bias correcting the CFS integration.

2.1.3 Anomaly Nesting

The process of anomaly nesting (Misra and Kanamitsu 2004) refers to the concept of removing the bias of the GCM before the downscaling process. This concept was inspired by previous studies, which showed that RCM simulations did not show significant advantages over the GCM simulations from which they were downscaled (Roads and Chen 2000), except in regions of complex topography (Roads and Kanamitsu. 2003). However, it has been shown that these errors associated with the RCM can be partially attributed to the systematic errors associated with the GCM (Pan et al. 2001, Noguer et al. 1998, and Druyan et al. 2002). The anomaly nesting process attempts to reduce the systematic errors of the GCM by replacing the model climatology with reanalysis climatology. This process reduces the drift of the GCM being used to feed the lateral boundary conditions of the RCM, thus reducing the errors in the RCM (Misra and Kanamitsu 2004).

For this study, the CFS JJA climatology is replaced with the climatology from the NCEP-NCAR Reanalysis I (atmosphere) and ERSSTv2 (SST) from the period 1950-1995. The CFS climatology is derived from the T62 33-year multidecadal coupled simulation (available from the CFS website, see: http://cfs.ncep.noaa.gov/). Bias corrections are applied to humidity, divergence, vorticity, and temperature at all verticals levels of the RSM (Chan and Misra 2009).

2.2 Comparison Data

The primary data used in this study are acquired from the Climate Forecast System Reanalysis (CFSR; Saha et al. 2010). CFSR is used to locate areas of significant model biases in precipitation and temperature. CFSR is also used to analyze model skill at predicting

above normal, normal, and below normal precipitation rates and temperatures. Finally, CFSR-derived correlation coefficients for three pairs of atmospheric variables are compared to model-derived correlation coefficients for the same three pairs of variables. Additionally, the TRMM and CMAP precipitation datasets are used to evaluate model skill at predicting precipitation rates.

2.2.1 Tropical Rainfall Measuring Mission (TRMM) 3B-43 Algorithm

The TRMM satellite was introduced in 2000 to help solve the problem of a largely under sampled tropical precipitation distribution. TRMM is focused on improving the understanding of the temporal and spatial distribution of tropical rainfall and latent heating (http://trmm.gsfc.nasa.gov/). The TRMM 3B-43 algorithm was designed to produce the Tropical Rainfall Measuring Mission (TRMM) and Other Data best-estimate precipitation rate and root-mean-square precipitation-error estimates. TRMM data are available as monthly averages on a 0.25° by 0.25° grid from 50°S to 50°N. Data are produced by combining the three-hourly merged high-quality/IR estimates with the monthly accumulated Climate Assessment and Monitoring System (CAMS) or Global Precipitation Climatology Centre (GPCC) rain gauge analysis (3A-45). The three-hourly merged data are summed for the calendar month, and then rain gauge data are used to apply a large-scale bias adjustment to the 3B-42 estimates over land (http://trmm.gsfc.nasa.gov/3b43.html).

2.2.2 CPC Merged Analysis of Precipitation (CMAP)

CMAP (Xie and Arkin, 1997) data are available globally in the form of monthly averages. CMAP is produced by merging precipitation estimates from microwave and infrared satellite algorithms, from rain gauges, and from model data. By merging the three data sources a more accurate representation of precipitation can be acquired than if any of the three sources were used individually. CMAP is available from 1979 onward though it is on a coarser grid (2.5° by 2.5°) than are the TRMM 3B-43 data (http://www.esrl.noaa.gov/psd/data/gridded/data.cmap.html).

2.2.3 Climate Forecast System Reanalysis (CFSR)

CFSR (http://cfs.ncep.noaa.gov/cfsr/) is a state-of-the-art high spatial and temporal resolution reanalysis data product. CFSR is available over the 31-year period between 1979 and 2009 in the form of hourly files and is available on a 0.5° by 0.5° horizontal grid with 37 vertical pressure levels for the atmosphere and 40 levels for the ocean (Saha et al. 2010). Aside from

higher spatial and temporal resolution, CFSR has three primary benefits over previous reanalysis, namely NCEP-NCAR R1 and R2: (1) coupling to the ocean during the creation of the six-hour guess field, (2) an interactive sea ice model, and (3) assimilation of satellite radiances for the entire period.

In this study, the primary variables acquired from CFSR are precipitation and two-meter temperatures. These variables are used to analyze the model skill during the dry season. Additionally, evaporation and incoming solar radiation are used to compare the correlations between the aforementioned three pairs of variables (correlations are described in Section 2.3.4).

2.3 Methods

The large-scale area of interest for this study is the South American continent and surrounding regions between 15°N and 40°S (RSM data is unavailable below 40°S) and between 30°W and 90°W. Two regions are of particular interest: the Amazon River Basin (ARB) and the subtropical region (ST) (Figure 2.1). The ARB is defined as the region between 4°N–17°S and between 45°W–75°W. The ST is defined as the region between 17°S–36°S and between 56°W–68°W.

2.3.1 Model Bias

The JJA, 2001–2007 climatological means of temperature (ºC) and precipitation (mm/day) are calculated for the three models and for the three comparison datasets. Models are compared to observations using percentage difference (*Diff*) calculations to isolate regions of significant bias.

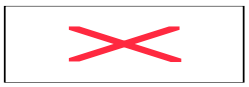

where $\bar{x}$ is the model climatological mean for a climate variable for ☒ ensemble members and ☒ years

$$\bar{x} = \frac{1}{NM}\sum_{i=1}^{N}\sum_{j=1}^{M} x_{ij}$$

and $\bar{j}$ is the observational climatological mean for the same climate variable for ☒ years.

$$\bar{j} = \frac{1}{N}\sum_{k=1}^{N} y_k$$

CFSR is used for precipitation and temperature comparisons, and TRMM and CMAP are used for precipitation comparisons only. Because this study uses a small sample size, statistical significance tests are applied to the differences. When these comparisons are conducted the comparison products are interpolated to the native grid of the model that they are being compared with. Statistical significance of the differences between datasets is tested using the student t test. Only values with greater than 90% significance are shown in this study.

2.3.2 Potential Predictability

In this study we will calculate the ratio of signal to total variance (the total variance equals the signal plus the noise) for two-meter air temperature and precipitation following Kumar and Hoerling (1995). For this study there will be M=6 ensemble members with N=7 years where the ensemble member is represented by *j* and the year is represented by *i*. The ensemble mean for a given climate variable for one model and for one year is then

$$\bar{x}_i = \frac{1}{M}\sum_{j=1}^{M} x_{ji} \quad .$$

The internal variance, or the spread around the ensemble mean for a particular year is then

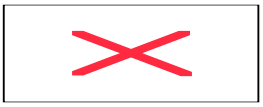

.

However, the spread can be dependent on the choice of year so we average the internal variance over all possible years and the result is referred to as noise.

The external variance, or the signal, is an estimate of the degree to which the difference between the ensemble mean forecast or different years is due to boundary conditions rather than to chance (Stefanova et al. 2010). The climatological ensemble mean for the particular variable is

$$\bar{x} = \frac{1}{N}\frac{1}{M}\sum_{i=1}^{N}\sum_{j=1}^{M} x_{ji},$$

and the external variance is given by

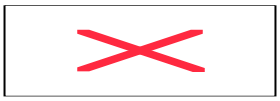

.

Finally, the total variance of the system is given by

By comparing the ratio of σ^2_{signal} to σ^2_{total} it can be determined which part of the observed signal is due to boundary conditions and which part is due to the uncertainty of the initial conditions. Larger ratios indicate more potential predictability of the climate variable. Values near one mean that the boundary conditions are overwhelming the effect of the noise, i.e., uncertain initial conditions, and values near zero indicate that the model is not "seeing" the boundary conditions, i.e., the entire signal is noise (Stefanova et al. 2010). However, large ratio values do not *necessarily* mean that forecasts will be skillful; thus, it is beneficial to examine the fidelity of the models further using a skill score such as the Relative Operative Characteristic (ROC) Curve.

2.3.3 Relative Operative Characteristic Curves

In this study we use the ROC curve (Mason and Graham 1999) to evaluate the ability of the three models to predict above normal, normal, and below normal precipitation and temperature. The ROC curve is developed using ratios that measure the proportion of events and nonevents for which warnings are issued or not issued. If we evaluate the model forecast as a probabilistic system (model forecast is either "yes" an event will occur or "no" an event will not occur, depending on the number of ensemble members that forecast an event to occur or not occur), we can construct a contingency table (see Table 2.1 adopted from Mason and Graham (1999)). From the contingency table we can acquire the aforementioned ratios, referred to as hit rate (ratio of hits to hits plus misses) and false alarm rate (ratio of false alarms to false alarms plus correct rejections). A hit can be described as follows: the model forecasts a "yes" and the observed is a "yes." A false alarm can be described as follows: the model forecasts a "yes" and the observed is a "no." A miss occurs when the model forecasts a "no" but the event actually occurs, and a correct rejection occurs when the model forecasts a "no" and the event does not occur. The ROC curve is constructed by plotting the scatter plot of hit rate vs. false alarm rate for each of the thresholds.

$$Hit\_Rate(HR) = \frac{h}{h+m} = \frac{h}{e}$$

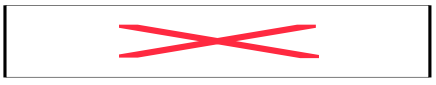

In our system, we have six ensemble members; thus, we have six thresholds. The threshold number (1-6) is the minimum number of ensemble members required to forecast a "yes" in order for the forecast system to declare a "yes." If the minimum number is not met then a "no" is declared.

The calculation of the area under the ROC curve (AUC) can be used as a measure of the skill of the model at forecasting an event. A more skillful model (a model has at least some skill if the AUC is > 0.5) will have the majority of the points on the curve clustered near the top left corner of the plot, where HR is close to 1 and FAR is close to zero. Therefore, a less skillful model will have more points clustered toward the bottom right corner of the plot and will have an AUC ≤ 0.5.

In this study, we evaluate the ability of the model to predict above normal, normal, and below normal precipitation rates (using TRMM, CMAP, and CFSR as observations) and temperatures (using CFSR as observations) over the ARB and over the ST (see Figure 2.1) independently. To accomplish this, we rank the area-averaged seasonal-mean precipitation or temperature into unequal terciles. The upper two (25%) years are labeled A, whereas the middle four years (50%) are labeled N and the lowest two years (25%) are labeled B. We perform the same unequal tercile ranking independently for the three models and include all six ensemble members. This means that there were 48 total cases for each model per region, resulting in 12 As, 24 Ns, and 12 Bs. Here we evaluate each model's predictability at varying sensitivities. Within the scope of this research, sensitivity can be defined as the minimum number of ensemble members in a given year that are required to correctly predict an event (either A, N, or B) in order for the model to forecast "yes." For precipitation we have three models, three observational datasets, two regions, and three events. This produces a total of fifty-four ROC curves. For temperature we produce a total of eighteen ROC curves. Additionally, we conduct a sensitivity experiment using a temporally longer integration of the CFS model. This integration consists of data from JJA between 1981 and 2003 and uses 15 ensemble members rather than 6. To test whether our model skill is reduced because we use only seven years and only six ensemble members we calculate ROC curves for temperature and for precipitation for the full 15-member integration and compare those results to the results from ROC curves calculated from a randomly-chosen group of six ensemble members. We also calculate ROC scores for a randomly-chosen group of seven consecutive years and compare those results to the results from

the ROC curves calculated with the full dataset. Temperature is evaluated against CFSR, and precipitation is evaluated against CFSR and CMAP.

2.3.4 Land-Atmosphere Feedback

We begin a cursory investigation into the land-atmosphere feedback in the models and compare these results with CFSR. Koster et al. (2003) split the land–atmosphere feedback into three parts (described in terms of wet anomalies): (1) wetting of soil by precipitation; (2) enhancement of evaporation by the wet soil; and (3) enhancement of precipitation by evaporation. Part one is obvious, and it cannot be denied that this interaction happens in nature. Part two can be supported by contemporaneous correlations of temperature and precipitation, which, in terms of wet anomalies, would be negative. The argument being that higher precipitation leads to more evapotranspiration and thus less sensible heat flux which in turn leads to lower temperatures (Koster et al. 2003). The third part of the feedback is more debatable, partly due to limited observations. Additionally, it is difficult to determine causality between a set of variables, which are highly interconnected (Misra and Dirmeyer, 2009). As a result, we can at best hope to offer a qualitative diagnostic of this part of the feedback cycle. To investigate this third part we follow Misra and Dirmeyer (2009) and calculate contemporaneous correlation coefficients between two pairs of variables: (1) evaporation and precipitation, and (2) downwelling shortwave flux and evaporation. Table 2.2 lists all three variable pairings we have just discussed and describes the information that can be inferred from the results. We conduct the three sets of correlations for each of the three models and compare the results with the same set of correlations from CFSR. When analyzing these results it is important to remember that correlations do not provide one with cause and effect, but merely suggest a relationship between two variables.

Table 2.1 Adopted from Mason and Graham (1999). Two-by-two contingency table for a binary forecast system

	Forecast		
Observations	Event Forecast: "yes" (W)	Event Forecast: "no" (W')	Total
Event (E)	Hit (h)	Miss (m)	e
Nonevent (E')	False alarm (f)	Correct Rejection (c)	e'
Total	w	w'	n

Table 2. 2 Lists of the pairs of variables between which correlation coefficients were calculated. The right column contains the intended purpose for conducting the correlation and the information that can be acquired from

Variable Pair	Purpose
Temperature w/ Precipitation	Negative correlations suggest that evaporative cooling due to precipitation reduces temperatures. Positive correlations suggest that evaporation is not contributing to precipitation (Koster et al. 2003).
Evaporation w/ Precipitation	Positive correlations indicate an arid climate regime, where precipitation is fed by local evaporative sources. Negative correlations indicate a non-arid regime (Misra and Dirmeyer, 2009).
Downwelling Short Wave Flux w/ Evaporation	Positive correlations indicate an *energy limited* regime. An energy limited regime is one in which plentiful moisture exists at the surface to fuel evaporation and evaporation is limited by the amount of radiation that reaches the surface. Negative correlations indicate a *moisture limited* regime, a regime in which evaporation rates are limited by the amount of moisture available at the surface rather than the amount of incoming solar radiation (Misra and Drimeyer, 2009).

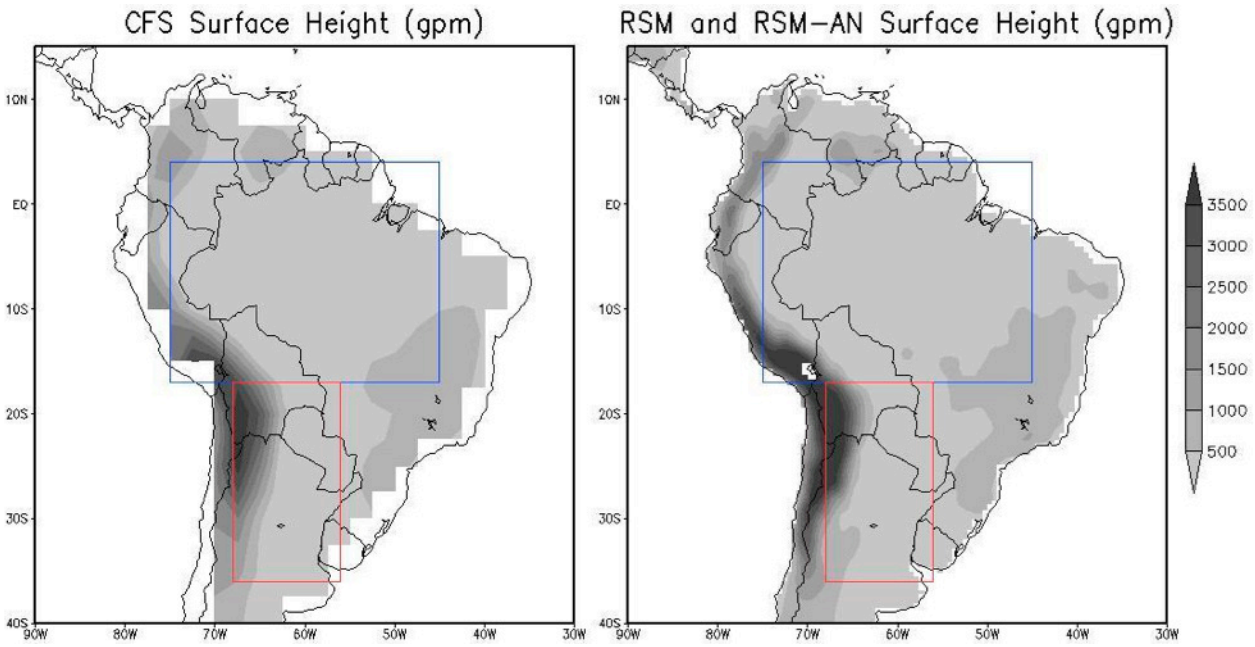

Figure 2. 1. The land area (shaded) and topography (GPM) for the NCEP CFS (left) and the NCEP Scripps RSM (right; and RSM-AN). The blue box represents the Amazon River Basin (ARB), and the red box represents the subtropical region (ST).

CHAPTER THREE

RESULTS

3.1 Dataset Comparison

In this study we primarily use CFSR for its long temporal range, its high resolution, and its large array of available variables. However, CFSR is produced with model influence, and thus is not free of error and bias. Hence, we compare CFSR with more widely used datasets, such as TRMM, CMAP, and CRU, to determine the location, magnitude, and sign of possible errors in the precipitation and temperature fields.

3.1.1 CFSR Two-Meter Temperature

Here, we compare CFSR two-meter temperatures averaged over JJA 2001–2005 with Climate Research Unit (CRU; http://badc.nerc.ac.uk/data/cru) two-meter temperatures averaged over the same time period. We cannot extend our temporal range through 2007 because CRU data are not available past 2006, which is also why we do not use CRU as a comparison dataset for our models. If we assume that CRU's temperatures are correct, we can use them to locate regions of error in CFSR. For this comparison, the CRU two-meter temperature field is bilinearly interpolated to the higher-resolution grid of CFSR.

CFSR and CRU temperatures are relatively similar over most of SA during the dry season. Differences between the two datasets are generally 1°C–2°C (Figure 3.1). Large differences occur over the elevated terrain of the Andes Mountains and the Guiana Highlands, where CFSR is approximately 4°C colder than CRU. The largest differences occur on the westward-facing slopes of the Andes Mountains. For most of the ARB, CFSR features colder temperatures than CRU does, except for the region around the Mato Grasso Plateau in Brazil and eastern Bolivia. CFSR is too warm throughout most of the ST, except for the region occupied by the Andes Mountains. Generally, CFSR has a cold bias over elevated terrain and a warm bias at lower elevations in the ST.

3.1.2 CFSR Precipitation Rate

We compare CFSR daily precipitation rates averaged over JJA 2001–2007 with CMAP and TRMM daily precipitation rates averaged over the same period. For this comparison, CMAP

and TRMM are bilinearly interpolated to the higher-resolution grid of CFSR. CMAP and TRMM are also both used as comparison datasets for the models. All three datasets have similar patterns of precipitation. Each shows distinct precipitation maxima within the ITCZ, and around 35°S (Figure 3.2). Precipitation rates drop off quickly south of the Guiana Highlands and are less than 1mm/day throughout most of the ARB and the ST in all datasets.

Differences between CFSR and CMAP (Figure 3.3; top), and between CFSR and TRMM (Figure 3.3; bottom) are nearly identical. Compared with CMAP and with TRMM, CFSR is wetter over the oceans, except immediately offshore. This negative tendency is slightly more pronounced when comparing CFSR with CMAP rather than with TRMM. CFSR appears to be drier within the ARB and wetter within the ST when compared to both CMAP and TRMM. The most striking difference between CFSR and the other two datasets lies within the ITCZ. In this region, CFSR has the tendency to produce greater than 6mm/day more precipitation than CMAP or TRMM. The ITCZ, however, does not impact either area of interest for this study, so we do not expect this large bias to affect our results.

Generally, CFSR accurately represents patterns and magnitudes of precipitation and temperature within the ARB and the ST when compared to TRMM, CMAP, and CRU. The largest temperature errors occur over mountainous terrain and the largest precipitation errors occur within the ITCZ. Although we cannot rectify these differences we must keep them in mind when we compare CFSR to the CFS, the RSM, and the RSM-AN. For completeness, we will also compare the models to CMAP and TRMM. Since CRU does not cover the entire temporal range of our model dataset, and since CFSR and CRU temperature fields are similar, we will not compare the models to CRU.

3.2 Model Comparison

3.2.1 Model Climatology

Figure 3.4 shows the JJA 2001–2007 average daily precipitation rates for the three models. The RSM and the RSM-AN produce distinct ITCZs and show precipitation rates increased over the northwest corner of the ARB. Additionally, both have precipitation maxima in the southeast corner of the ST and lower precipitation rates in the northwest corner. The CFS has a distinct ITCZ; however, there is almost no maximum in precipitation over the northwest corner

of the ARB and no distinguishable precipitation maximum in the southeast corner of the ST. The RSM is clearly producing the most precipitation, whereas the CFS is clearly producing the least.

Figure 3.5 shows the JJA 2001–2007 averaged two-meter air temperature for the three models. As was the case with the precipitation plots, the RSM and RSM-AN are spatially similar, whereas the CFS is drastically different. The RSM and RSM-AN both display temperature maxima just south of the equator near the center of the ARB. The RSM-AN maximum (~29°C) appears to be about 2°C warmer than the RSM maximum. The CFS, however, is warmer than both the RSM and RSM-AN. Much of the ARB in the CFS is occupied by >29°C temperatures. If precipitation and temperature are strongly linked through evaporative cooling then this phenomenon is understandable (i.e., the CFS produces the least precipitation and thus has the highest temperatures, whereas the RSM produces the most precipitation and has the lowest temperatures). In the ST, all three models display temperature minima of <11°C in the western and southwestern regions where there is elevated terrain, as well as decreasing temperatures from north (~22°C in southern Bolivia) to south (<11°C in central Argentina).

3.2.2 Model Bias

In this section, we compare the models' JJA 2001–2007 average precipitation rates to CFSR, TRMM, and CMAP precipitation rates, and we compare the model's JJA 2001–2007 two-meter air temperatures to those of CFSR.

When compared to CFSR precipitation rates (Figure 3.6), the CFS and RSM-AN precipitation rates are primarily negatively biased within the ARB, except over elevated terrain. The CFS's area-averaged bias is ~-1.1mm/day and the RSM-AN's area-averaged bias is ~-0.7mm/day. The RSM exhibits a positive bias (~0.9mm/day) in all areas except for northeastern Brazil. In the ST, the CFS and the RSM-AN display similar patterns of bias: negative bias in the eastern half of the box over the lowlands of Argentina, and positive bias in the western half of the box over the Andes Mountains (CFS~-0.4mm/day, RSM-AN~-0.1mm/day). The RSM is mostly positively biased and has an area-averaged bias of ~0.2mm/day. The fact that the RSM-AN precipitation more closely resembles the precipitation produced by the CFS than that produced by the RSM is a puzzling result. Our results suggest that the RSM-AN potentially retains more of the CFS's bias than the RSM does, particularly over the ARB. Although it is beyond the scope of this research to do so, it is suggested that this result be investigated further.

A similar pattern of bias is observed when the three models are compared to TRMM (Figure 3.7) and CMAP (Figure 3.8). In both cases, the CFS and RSM-AN are negatively biased over the ARB and ST. When compared to both TRMM and CMAP, the RSM display similar patterns of positive and negative bias in the ARB and the ST. The results of the comparisons with CFSR, TRMM, and CMAP indicate that the models are generally negatively biased in the ARB, with the RSM having the smallest bias of the three models and in some instances actually exhibiting a positive bias. In the ST, all three models are positively biased over the Andes Mountains and negatively biased over the lower terrain of Argentina.

The models' JJA 2001–2007 two-meter temperature field is compared to the same field from CFSR only. However, as discussed in Section 3.1.1, CFSR and CRU temperatures are fairly similar, with most points inside the ARB and ST exhibiting mean temperature differences of less than ± 2°C. Figure 3.9 shows that the RSM temperature field is most similar to CFSR temperature field. In the ARB, the RSM has a bias of ~0.01°C, whereas the CFS and RSM-AN exhibit positive biases of 3.5°C and 0.9°C, respectively. In the ST, the CFS and RSM-AN no longer exhibit the same pattern. Here, the CFS is negatively biased (~-1.5°C), whereas the RSM (~0.6°C) and RSM-AN (2.1°C) are both mostly positively biased. As we can see, the RSM, again, has the smallest bias.

3.3 Signal-to-Noise Ratio

The potential predictability of dynamical seasonal ensemble forecasting is based on the premise that long-term predictability is associated with slowly varying surface boundary conditions (primarily SSTs) that remain nearly constant between ensemble members. The potential predictability stems from the fact that atmospheric anomalies are largely governed by boundary condition/SST anomalies (Stefanova et al. 2010). By comparing the ratio of the variance of the external forcing (i.e., the boundary conditions or SSTs) to the total variance, we can arrive at the potential of predictability within the modeling system. Larger ratios mean that the system is more easily distinguishing between different regimes associated with different boundary conditions. Smaller ratios mean that the internal variance is overwhelming the signal of the boundary conditions and that the model has more difficulty distinguishing between different regimes. It is important to point out that despite its name, potential predictability ratio, a larger

ratio value in a particular location does not necessarily mean that the model will have more skill in that region over another.

Figure 3.10 shows the ratio of the signal to the total variance of precipitation for the three models. At best, the models display scattered regions of ratio values greater than the threshold of 0.5 in the ARB and the ST. However, the CFS and the RSM display some patchy areas of larger ratio values in the northern and eastern portions of the ARB, whereas the RSM-AN displays some higher values in the northern portion only. There are almost no values greater than 0.5 in the ST in any of the models. The spotty areas of higher potential predictability observed in the ARB seem to coincide with more seasonal precipitation (see Figure 3.4) over higher topography or within the ITCZ. Although most of the precipitation that falls in the ARB is convective, and is thus generally considered "noisy," areas with *persistent* convective precipitation can still produce a high signal. Most likely, this is what causes the spotty areas of high potential predictability in the ARB.

All of the models display larger ratios in the ARB for two-meter temperature than they do for precipitation (Figure 3.11). However, there is still little potential predictability in the ST in any of the models. The RSM and the RSM-AN display larger ratios than the CFS in both the ARB and the ST. In the ST, the CFS does not display any values greater than 0.5, whereas the RSM and RSM-AN have several small regions where the ratio is greater than 0.5. As discussed in Section 3.2.2, the CFS two-meter air temperature field also exhibits the largest bias when compared to CFSR's temperatures. Although large bias does not necessarily mean low potential predictability or low ensemble forecast skill, it could be an early indicator of such a problem. The fact that temperature has a greater potential predictability than precipitation is not surprising, as temperature is generally a much less "noisy" field. The only way to get an exact measure of the model's ensemble forecasting skill is to calculate the area under the ROC curve, which will be discussed in the Section 3.4.

3.4 Model Skill

The calculation of the AUC is our chosen measure of model skill because it is an efficient way of evaluating ensemble forecasts. In this study, we use ensemble forecasting to predict positive and negative anomalies, as well as neutral conditions, of temperature and precipitation.

As was discussed in Section 2.3.3, ensemble forecasting requires a critical number of ensemble members to agree on a solution before it can be declared that such a solution will or will not happen. There are three primary objectives we hope to achieve through our ROC curve analysis. First, we would like to know if any of the three models possess some skill (i.e., AUC > 0.5) in predicting below normal, normal, and/or above normal temperatures and precipitation. The three aforementioned conditions are referred to as *events* throughout this study. Second, we wish to determine if either the downscaling process or the anomaly nesting process improves the skill of the forecasts. The first two objectives will be discussed in Section 3.4.1 (precipitation) and in Section 3.4.2 (two-meter air temperature). Lastly, using a longer integration of the CFS (1981–2003) consisting of 15 ensemble members, we seek to determine whether using only six ensemble members and/or only seven years causes us to underestimate or overestimate the skill of the models.

The results of the AUC calculations are illustrated in Figures 3.12–3.19. Generally, the models display higher forecast skill in the ARB than they do in the ST, and temperature forecasts are more accurate than precipitation forecasts. This corresponds well with the results from Section 3.3; recall that temperature had more potential predictability than precipitation and that the ARB had more potential predictability than the ST.

3.4.1 Precipitation

Using CFSR as the comparison dataset, the RSM-AN has the highest skill of the three models for all events in the ARB (Figure 3.12). The RSM has the same skill as the CFS when predicting below normal and normal precipitation, but has zero skill predicting above normal precipitation, whereas the CFS has some skill for this event. In the ST, all three models exhibit little skill (Figure 3.13). The CFS has zero skill predicting any of the three events, whereas the RSM has some skill predicting normal and above normal events and the RSM-AN has some skill predicting normal events only. These results lead us to believe that in the ARB there is little benefit to the downscaling process alone, but when it is coupled with the anomaly nesting process there is a distinct improvement in forecast skill over the CFS. In the ST, there is some benefit to the downscaling process but no added benefit from the anomaly nesting process.

We see slightly different results when we do the same ROC curve analysis using CMAP as our comparison dataset. The most glaring feature is the poor consistency between the AUC scores achieved using CFSR and the scores achieved using CMAP. Although slight differences

in the ROC curves were expected to occur as a result of inherent differences in the datasets, the magnitude of the differences and the impact these differences could have on future uses of the models is striking. For example, when we compare the models to CFSR, only the RSM fails to achieve some skill at predicting all three events in the ARB. However, when compared to CMAP, none of the three models are able to achieve skill with all three events combined (Figure 3.14). In fact, only the RSM-AN achieves some skill predicting more than one event (it achieves skill forecasting above normal and below normal events). Despite this dissimilarity, when we use CMAP as our comparison dataset, we still find the RSM-AN to possess the highest skill.

A similar scenario appears in the ST when we use CMAP as our comparison dataset; the AUC scores are not similar between CFSR and CMAP. However, the RSM still possesses the most skill (Figure 3.15). An additional difference is that rather than predicting normal and below normal events with some skill, as it did with CFSR, the RSM predicts only below normal events best with CMAP.

The fact that we see slightly different results when we use different comparison datasets shows us how sensitive skill score tests can be. Of course, the model data used in the ROC curve calculation is not changing when we use a different comparison dataset; thus, changes in the results are due to differences in the comparison data. In the case of ROC curves, the exact value forecast by the model for a particular year is not of upmost importance. Rather, whether that value is above or below normal relative to other years in the model and whether that ranking matches the ranking given to that same year by the comparison dataset takes precedence.

The results of the ROC curves using TRMM are, in some respects, more similar to the results of CFSR than to those of CMAP. As is the case with CFSR, the only event in any of the models that does not show signs of being skillfully predicted is above normal precipitation using the RSM (Figure 3.16). Unlike CFSR and CMAP, TRMM leads us to believe that there is no benefit to the downscaling or anomaly nesting processes in the ARB. In this comparison, the CFS has the most skill predicting below normal precipitation and has the same amount of skill as the RSM-AN predicting normal and above normal precipitation. Interestingly, the RSM-AN has much less skill predicting below normal precipitation and more skill predicting normal precipitation when TRMM is used as the comparison dataset rather than CFSR or CMAP. Again, this is an artifact of the ranking given to the years used in the observational datasets (2001–2007), in terms of their mean seasonal precipitation rates. The ranking of particular years in the

different datasets can be found in Appendix A. Appendix A shows that the rankings in different comparison datasets are similar. Finally, in the ST, when TRMM is used for comparison data, the RSM displays the most skill (Figure 3.17). Therefore we are again concluding that there is a benefit to downscaling in the ST but no added benefit from the anomaly nesting process.

3.4.2 Two-Meter Temperature

To estimate the model skill for above normal, normal, and below normal temperature events, we calculate ROC curves using CFSR only. In the ARB, the RSM-AN has the most skill predicting all three events (Figure 3.18). The RSM has the next highest skill for normal and above normal temperature events, though it has no skill predicting below normal events. The CFS has the least skill predicting normal and above normal events, but unlike the RSM it exhibits some skill predicting below normal events. In this case, it is evident that by applying the downscaling and anomaly nesting processes we will achieve greater predictability. If we apply the downscaling only, we can improve the forecasts of normal and above normal events but not below normal events.

In the ST, the results are far less definitive. The CFS displays some skill forecasting above normal events only, the RSM-AN displays significant skill forecasting below normal events only, and the RSM displays no skill with any of the events (Figure 3.19). In this situation, we do not believe that there is enough information to make conclusions regarding how downscaling and anomaly nesting affect our results.

3.4.3 Sensitivity Experiment

Here we examine the third objective of our ROC curve analysis, which is to show whether the models are limited by their small temporal range and few ensemble members, by using a longer integration of the CFS (1981–2003) with more ensemble members (15 instead of 6). We can conclude whether the low number of ensemble members has an effect on our results by calculating ROC curves for the full 15-member CFS and then by conducting a second set of curves for which we use only 6 randomly selected ensemble members. To determine whether the small number of years is impacting our results, we conduct a similar experiment. Here we compare the 23-year, 15-member CFS with the same 15-member CFS consisting of a randomly chosen seven consecutive years. The major limiting factor in this experiment is that it is difficult to determine if the random selection is representative of the dataset as a whole. We exclude TRMM from this comparison because it does not offer data for all 23 years.

When we use CFSR to evaluate precipitation in the ARB, we see that the skill for all three events changes little when we reduce the number of ensemble members (Figure 3.12). The skill for normal and above normal precipitation events increases slightly, while the skill for below normal events decreases slightly. A similar pattern is observed in the ST, as little change in skill is observed between the 15-member CFS and the randomly chosen 6-member CFS (Figure 3.13). In the ST the skill of above normal and below normal precipitation decreases, whereas the skill for normal precipitation increases. As is the case with the primary three models, there is generally higher predictability of events in the ARB than in the ST.

As was the case when we used CFSR, when we use CMAP as our comparison dataset little changes when we reduce the number of ensemble members. In the ARB, when we decrease the number of ensemble members, the skill of all three events decreases slightly (Figure 3.14). In the ST, there is little skill possessed by either the 15-member CFS or the random-6-member CFS (Figure 3.15). The 15-member CFS has some skill predicting below normal events only and the random-6-member CFS has some skill predicting above normal events only.

Overall, it appears that when we limit the number of ensemble members we do not necessarily limit, or artificially inflate the skill of the model when predicting precipitation.

When we limit the number of ensemble members used to predict two-meter air temperature we see slightly larger changes than we did for precipitation. In the ARB, it does appear that when we limit the number of ensemble members we may be limiting the potential skill of the model. Here, the skill of all three events drops and the skill of the normal temperature event actually falls below the threshold of 0.5 (Figure 3.18). There also appears to be a slight loss of skill in the ST when we reduce the number of ensemble members. Here, the normal events had no skill in either the 15-member or the 6-member CFS, the skill of the above normal events did not change, and the skill of the below normal events dropped significantly (Figure 3.19).

For both two-meter air temperature and precipitation we see obvious changes in the results of our ROC curves between the 15-member CFS with 23 years and the 15-member CFS with only 7 years (Figures 3.12, 3.13, 3.18. and 3.19). This result tells us that we may be overestimating or underestimating the skill of the primary three models by using only seven years. It is impossible to know whether we are overestimating or underestimating simply by conducting one test. A more thorough investigation would be needed. As is often the case with

statistical skill scores, using a longer dataset could yield a more significant representation of the models' skill.

3.5 Land-Atmosphere Feedbacks

The final aspect of this project is to determine how the land and the atmosphere interact in the three models, and then to determine if those results match the results from CFSR. The purpose of this investigation is to provide a potential reason why the models are less than perfect per the results of Section 3.4.

3.5.1 Models

As discussed in Section 2.3.4, the second part of the land-atmosphere feedback can be illustrated with contemporaneous correlations between precipitation and temperature. The results of this test in all three models are similar. In the ARB, the northern portion of the box is mostly negative, whereas the southern portion is weakly positive (left panel of Figures 3.20, 3.21, and 3.22). This implies that in the northern portion of the box, precipitation is wetting the soil and then being evaporated, reducing the sensible heat flux and cooling the air through the evaporative cooling process, and possibly leading to future precipitation. In the RSM, the negative correlations occupy a slightly larger portion of the box than they do in the RSM-AN and CFS. In the southern portion, the results suggest that surface evaporation is not leading to precipitation; otherwise, we would have negative correlations (Koster et al. 2003). In the ST, correlations are very weakly positive or negative and no distinct spatial pattern exists.

The third part of the cycle, the enhancement of precipitation by evaporation, is explained by the last two sets of correlations. All three models exhibit positive correlations between flux and evaporation in both the ARB and the ST (middle panel of Figures 3.20, 3.21, and 3.22). This indicates that in SA during the dry season evaporation is energy limited (Misra and Dirmeyer 2009). The term energy limited implies that there was not enough incoming solar radiation to evaporate all of the moisture at the surface. This result agrees well with what we see in the correlation plots between evaporation and precipitation.

Spatially the correlations of evaporation with precipitation are similar to correlations of temperature with precipitation. Most areas display negative correlations except for the southern portion of the ARB where values are weakly positive (right panel of Figures 3.20, 3.21, and

3.22). Negative values are a mark of aridity, which means that there is significant evaporation but little precipitation. Because evaporation has been limited by the lack of radiation, the atmosphere is not absorbing enough moisture to support precipitation. It is likely that too much of the model domain is in an arid regime as a result of the models producing less precipitation than is actually observed (Figures 3.6, 3.7, and 3.8). This result, however, conflicts with our interpretation of the correlations between temperature and precipitation. From that plot, we concluded that evaporation results in precipitation and thus evaporative cooling, because we saw that when precipitation increased, temperature decreased. We now show that evaporation does not always lead to precipitation. Without conducting a full moisture budget, we cannot determine exactly why we see this result. One hypothesis is that local recycling is not important during the dry season in the models. The model is evaporating a significant amount of moisture and the evaporation process is acting to cool the near-surface air. However, the amount of evaporation is not enough to produce precipitation. Instead, precipitation is fed by moisture that is advected from remote locations.

3.5.2 CFSR

When the same sets of correlations are performed with CFSR, the results are similar to those obtained from the suite of models. Figure 3.23 (left panel) shows that the correlation pattern between evaporation and precipitation is spatially similar to the pattern produced by the models. It shows negative correlations in the northern portion of the ARB and weak positive values in the southern portion. These results indicate that evaporation probably fuels precipitation in the northern part of the ARB, but not in the southern portion. Correlation coefficients in the ST region are a mix between weak positive and weak negative values. As was the case in the models, CFSR shows mostly positive correlations between downwelling shortwave flux and evaporation in the ARB, meaning evaporation is energy limited (Figure 3.23, middle panel). In the ST, however, there is a small region where correlations are negative; thus evaporation is moisture limited. The largest differences between the models and CFSR occur in the correlations of evaporation and precipitation. Unlike the models, CFSR shows primarily positive correlations between these variables in both the ARB and the ST. This means that CFSR is indicating that SA is a nonarid regime during the dry season, whereas the models are saying SA was an arid regime. Additionally, it means that evaporation is leading to precipitation, which,

unlike the results seen in the models, is in agreement with the correlations of precipitation and temperature.

As discussed in Section 3.5.2, explaining why the models suggest that evaporation leads to precipitation in one plot and contradicting that statement with another plot would require a full moisture budget analysis and is beyond the scope of this research. We would also need a moisture budget analysis to determine why evaporation seems to play more of a role in precipitation in CFSR than in the models. It is important to remember that correlations due not necessarily imply cause and effect and that our interpretations of the correlations we have presented are based on previous studies.

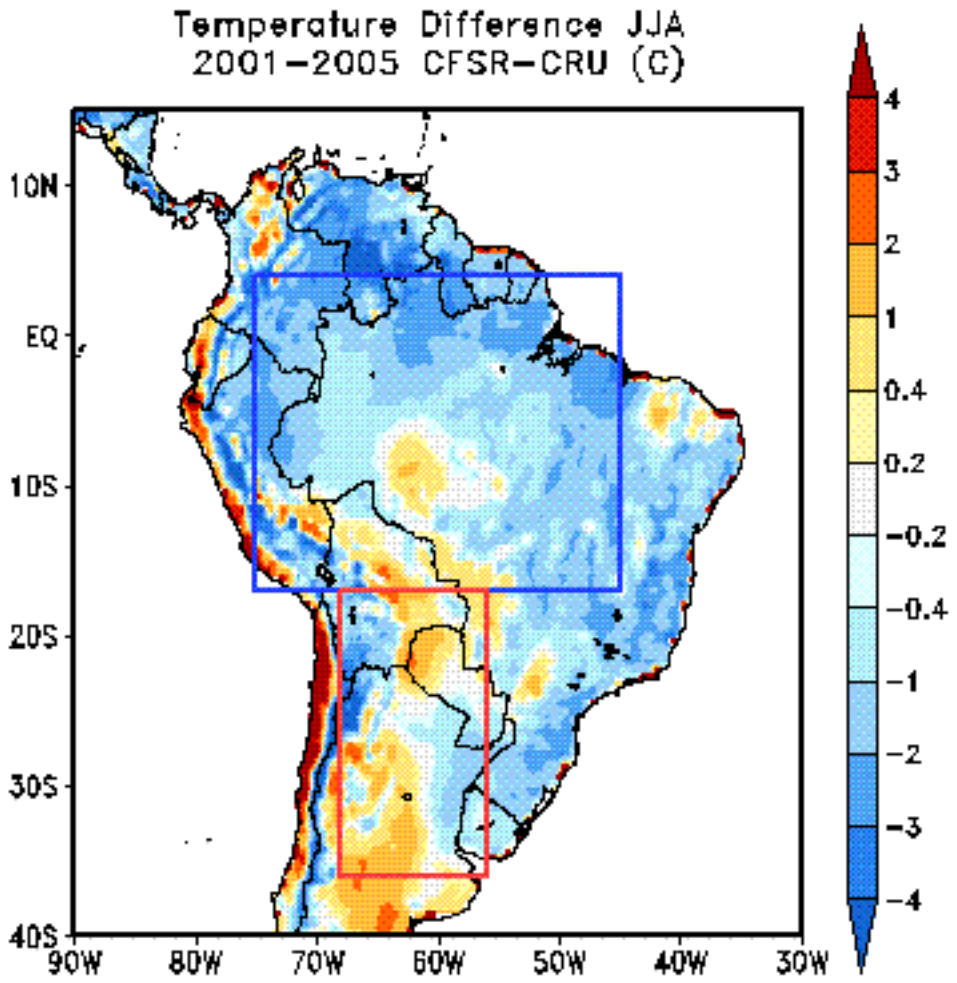

Figure 3.1 The difference in two-meter air temperature between CFSR and CRU in degrees Celsius. Temperatures are an average over JJA from 2001 through 2005. As in Figure 2.1 the blue box represents the ARB and the red box represents the ST. Values over bodies of water are masked out. The statistical significance test was not applied to this image.

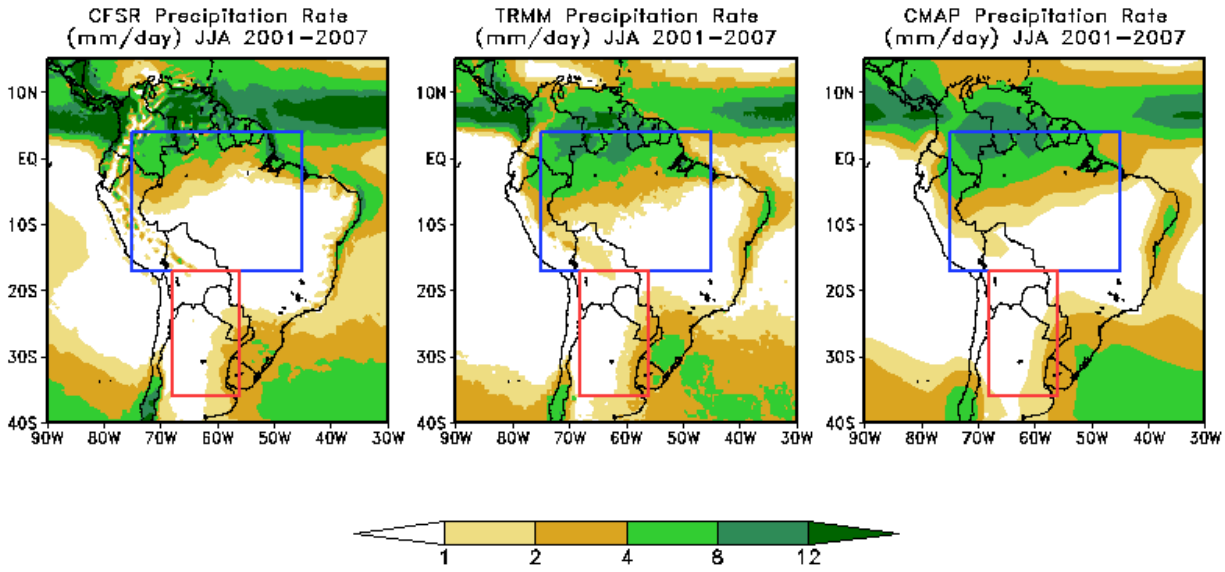

Figure 3.2 Precipitation rate averaged over JJA 2001–2007 for CFSR (left), TRMM (middle), and CMAP (right). Units are in mm/day.

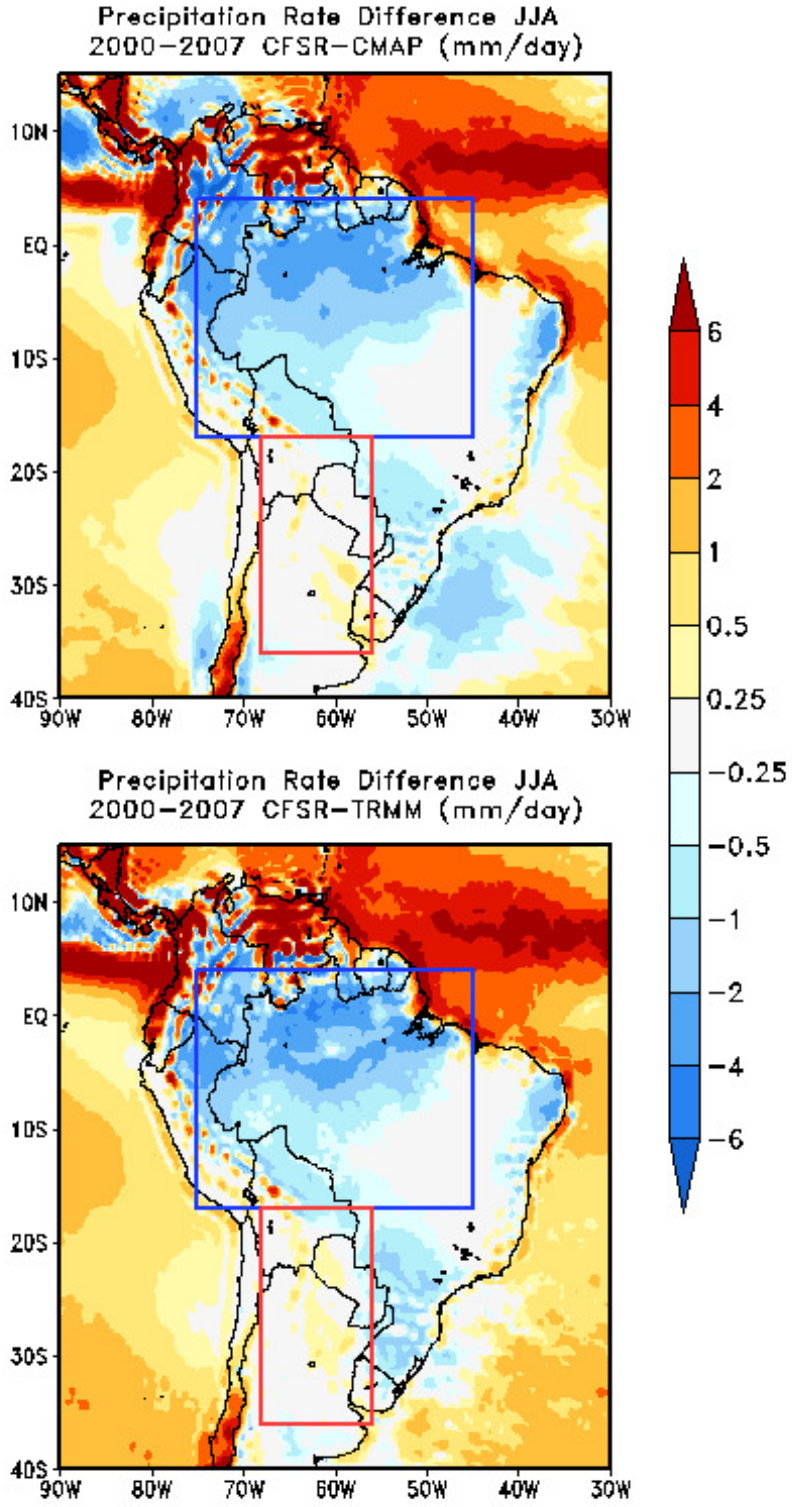

Figure 3.3 Difference between the 2001–2007 JJA averaged precipitation for CFSR minus CMAP (top) and CFSR minus TRMM (bottom). Units are in mm/day. The statistical significance test was not applied to these differences.

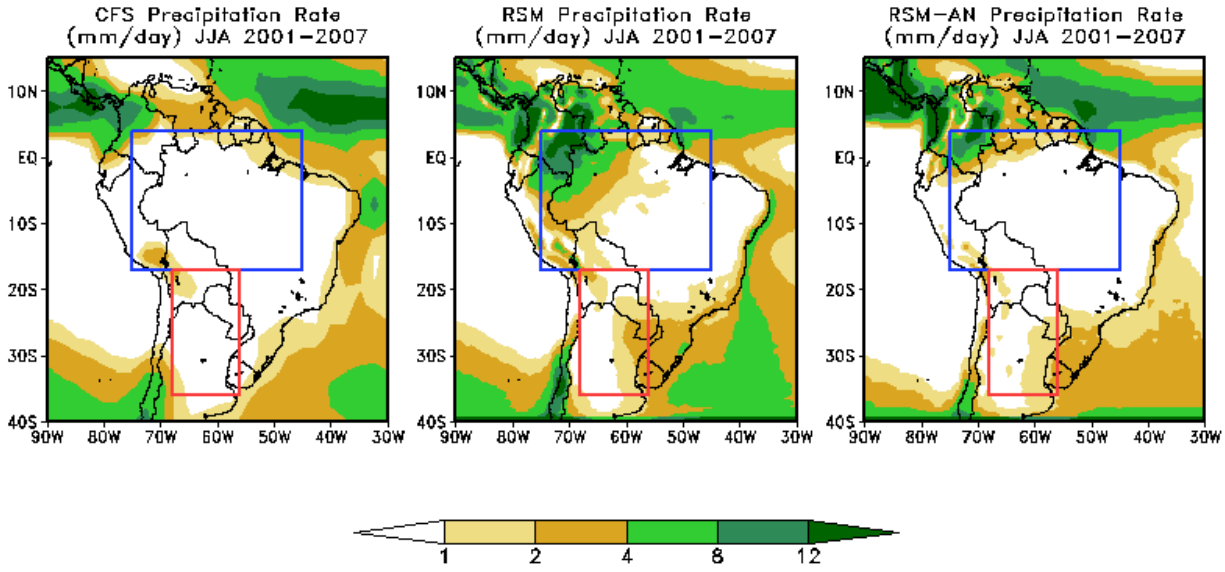

Figure 3.4 Precipitation rate averaged over JJA 2001–2007 for CFS (left), RSM (middle) and RSM-AN (right). Units are in mm/day.

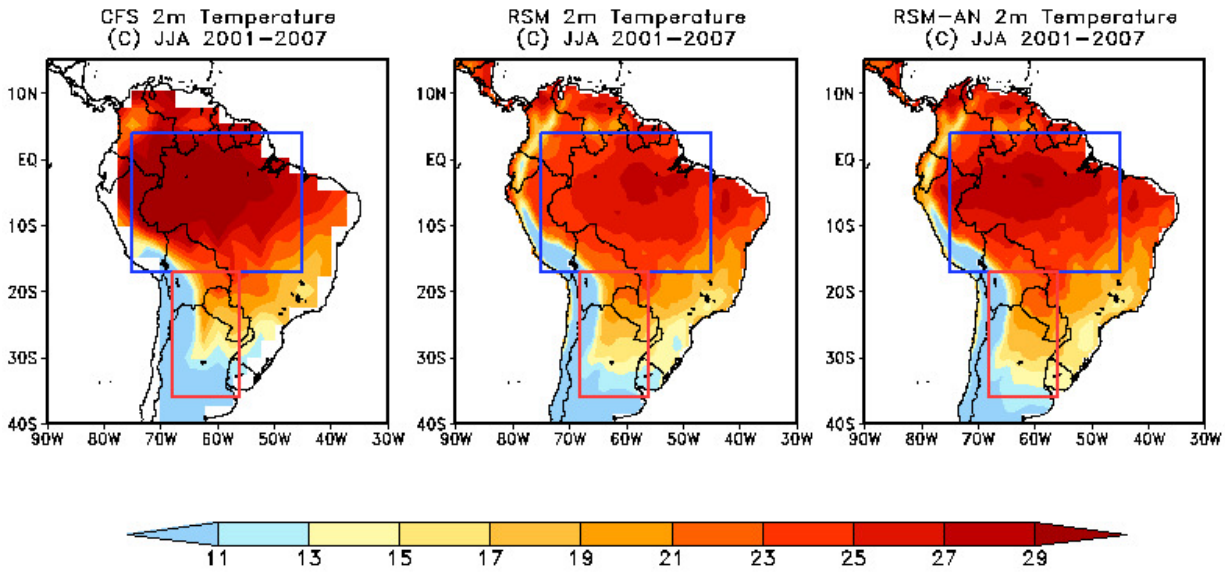

Figure 3.5 Same as Figure 3.4 except for two-meter air temperature and units are in degrees Celsius.

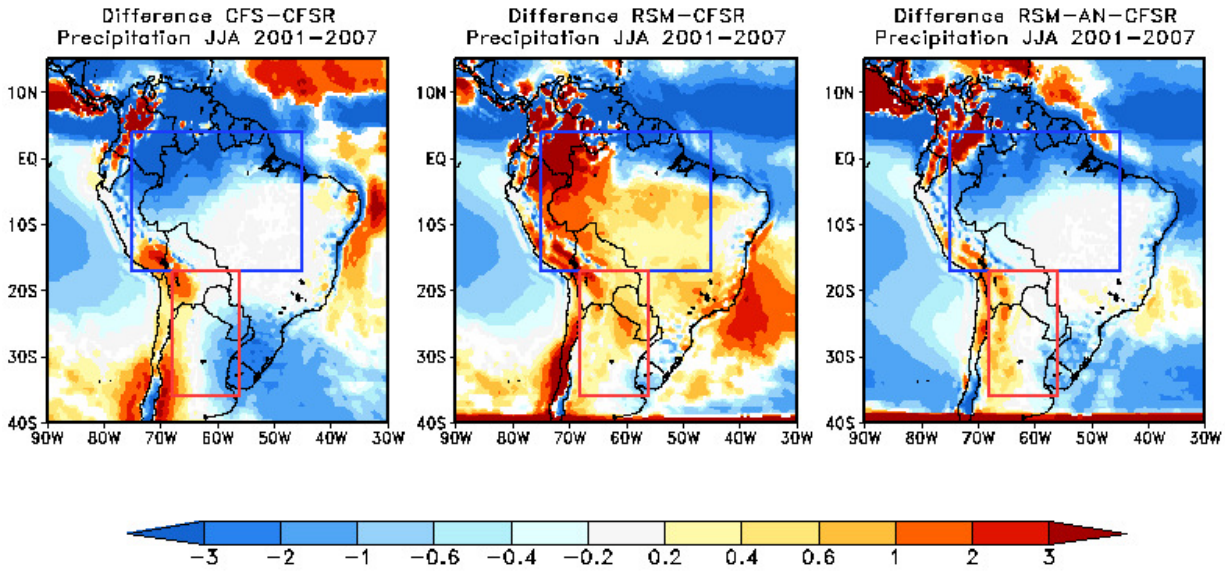

Figure 3.6 Difference between the JJA 2001–2007 average precipitation rates for the models and CFSR. CFS minus CFSR is on the left, RSM minus CFSR is in the middle, and RSM-AN minus CFSR is on the right. To conduct grid-point to grid-point differences the models are interpolated to the higher-resolution grid of CFSR. Units are in mm/day. Positive differences indicate that the model rains more than CFSR and negative differences mean the model rains less than CFSR. Regions that do not meet the 90% confidence level of the student t-test are masked out in white.

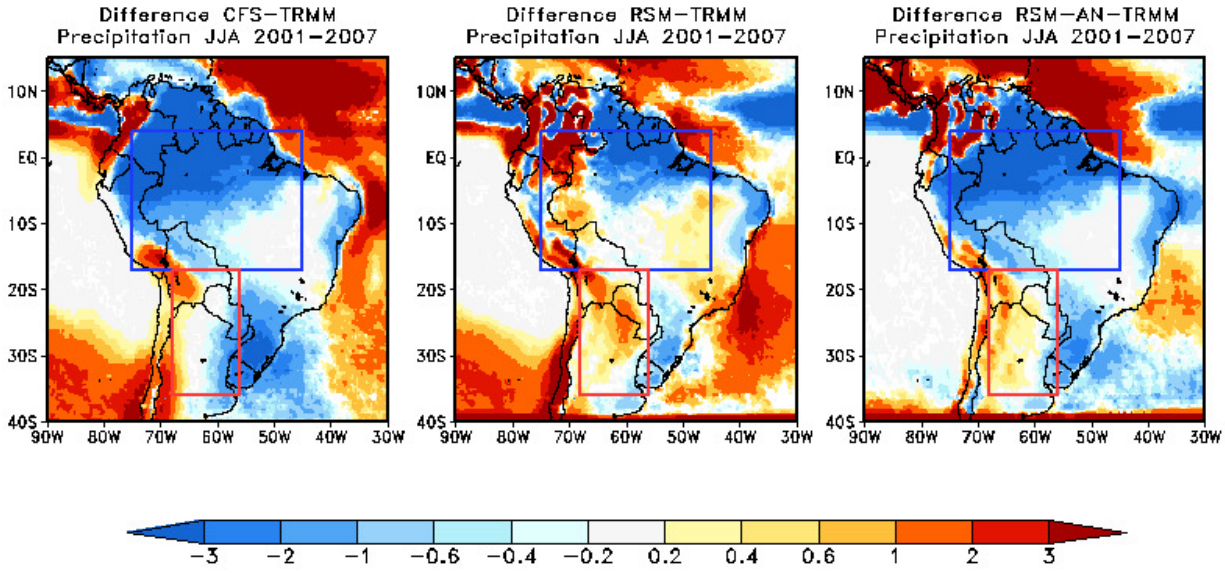

Figure 3.7 Same as Figure 3.6 except for the differences are now between the models and TRMM.

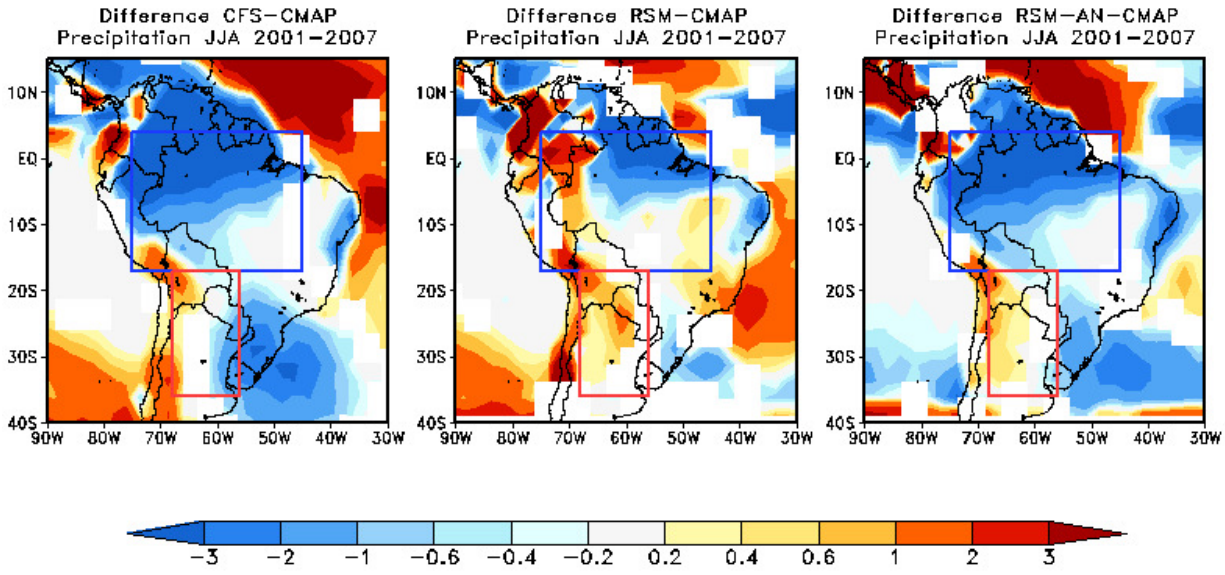

Figure 3.8 Same as Figure 3.7 except differences are now between CMAP and the models.

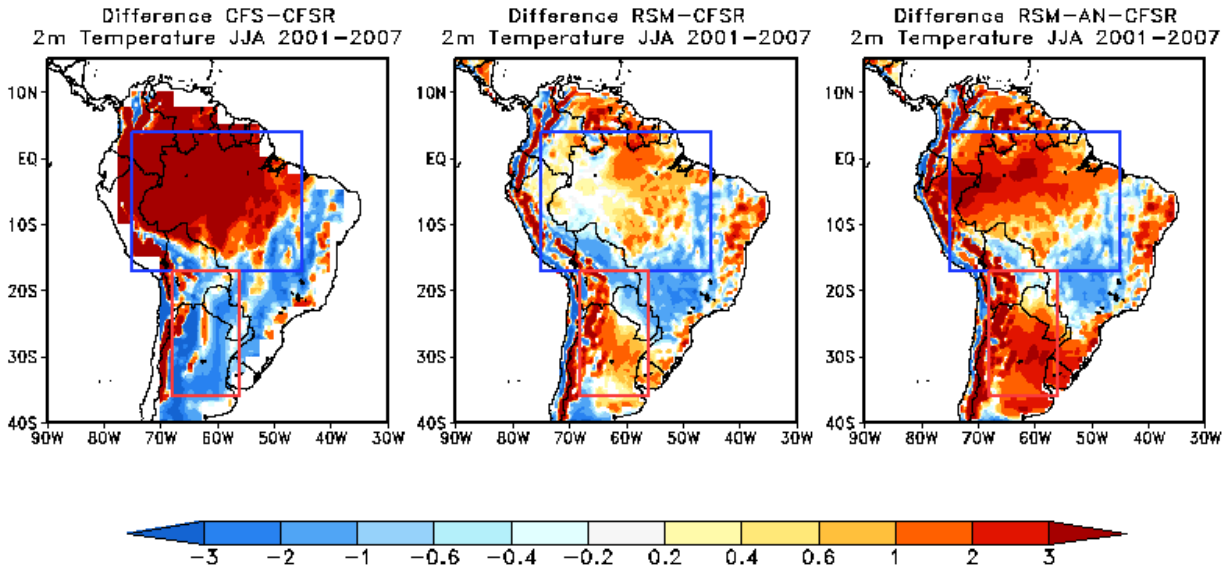

Figure 3.9 Same as Figure 3.6 except the differences are now for two-meter air temperature. Grid boxes over water are masked out and are not necessarily insignificant.

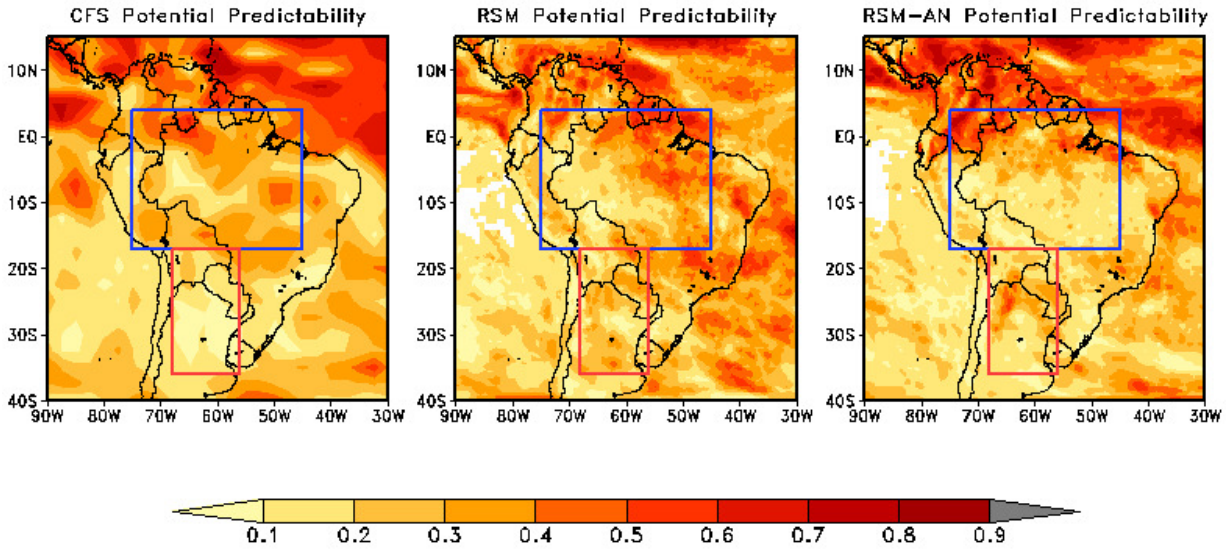

Figure 3.10 The ratio of the signal to the total variance or, potential predictability, for the six ensemble members from 2001–2007. CFS is on the left, the RSM is in the middle, and the RSM-AN is on the right. Where larger values are observed, the model should exhibit more skill in forecasting precipitation events. In the RSM and RSM-AN, regions in the western Pacific Ocean that show up in white are areas where the model did not produce any precipitation and the calculation of the potential predictability was undefined (i.e., division by zero occurred).

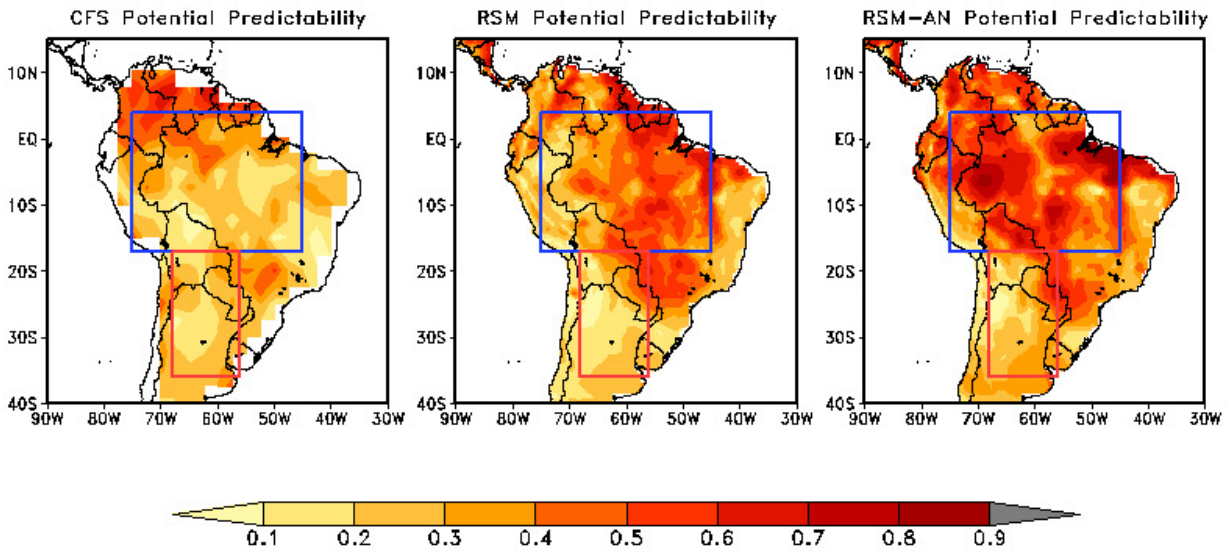

Figure 3.11 Same as Figure 3.10 except showing the potential predictability of two-meter air temperature.

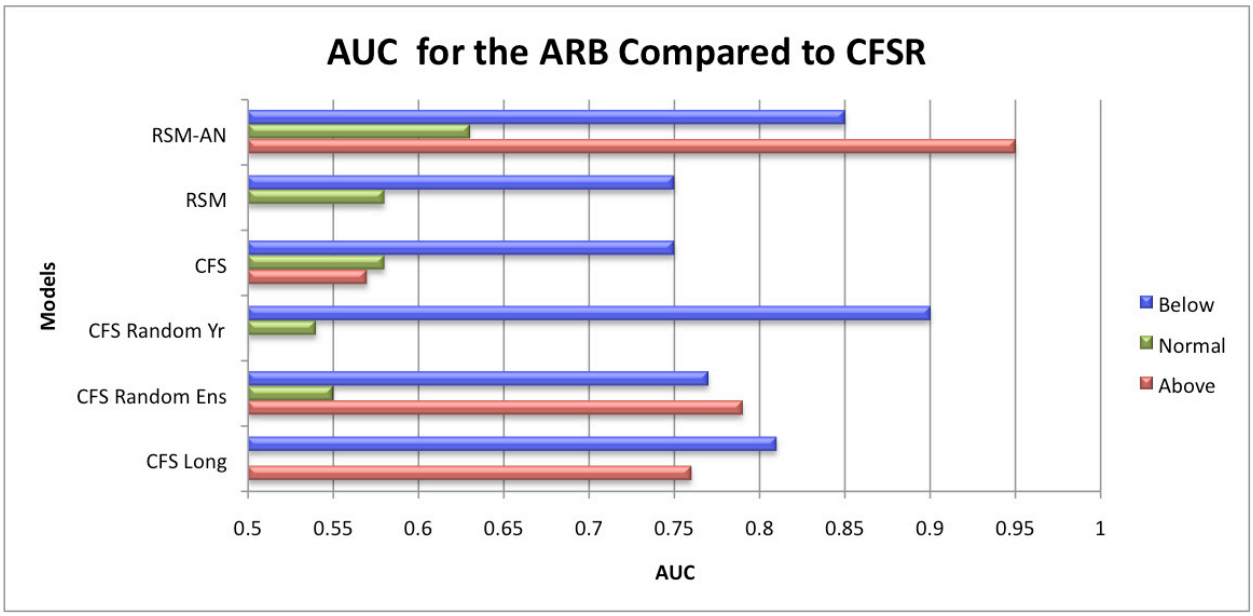

Figure 3.12 Bar graph depicting the area under the ROC curves calculated for above normal (red), normal (green), and below normal (blue) precipitation events using CFSR as the comparison dataset for the ARB region. The three primary models (CFS, RSM, and RSM-AN) are shown along with the CFS integration including 23 years and 15 ensemble members (CFS Long), the same 23 year integration consisting of a randomly chosen 6 ensemble members (CFS Random Ens), and the same CFS integration with 15 ensemble members but consisting of only 7 randomly chosen (1997 through 2002) consecutive years (CFS Random Yr). Only AUCs greater than 0.5 are shown because values less than that indicate that the model has no skill.

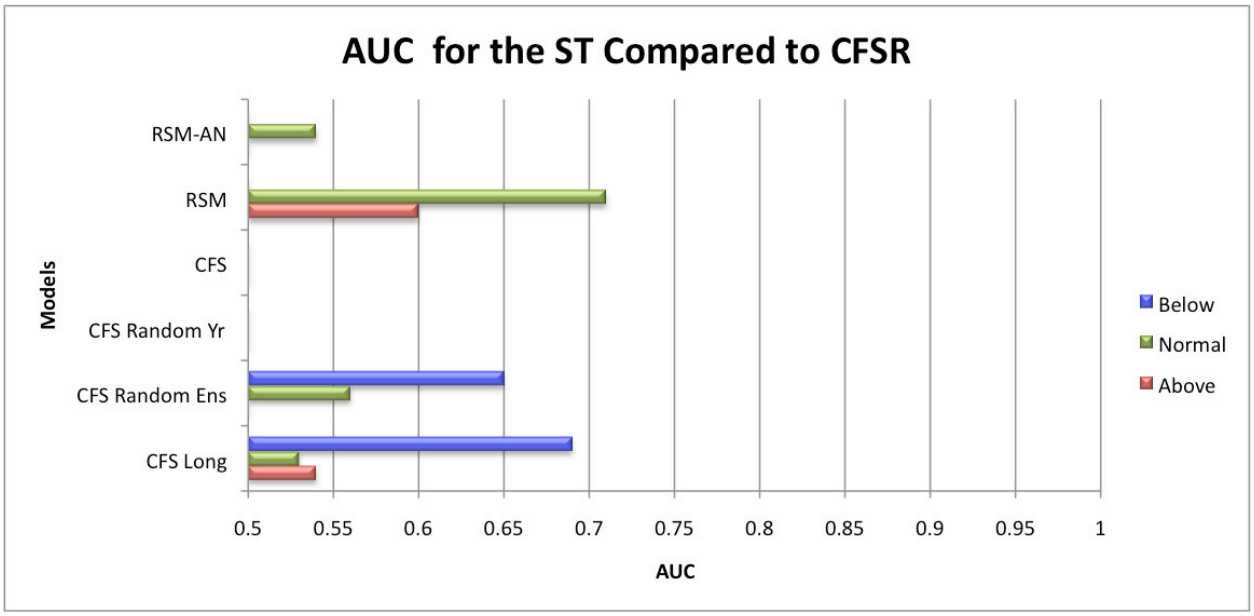

Figure 3.13 Same as Figure 3.12 except the region has changed to the ST.

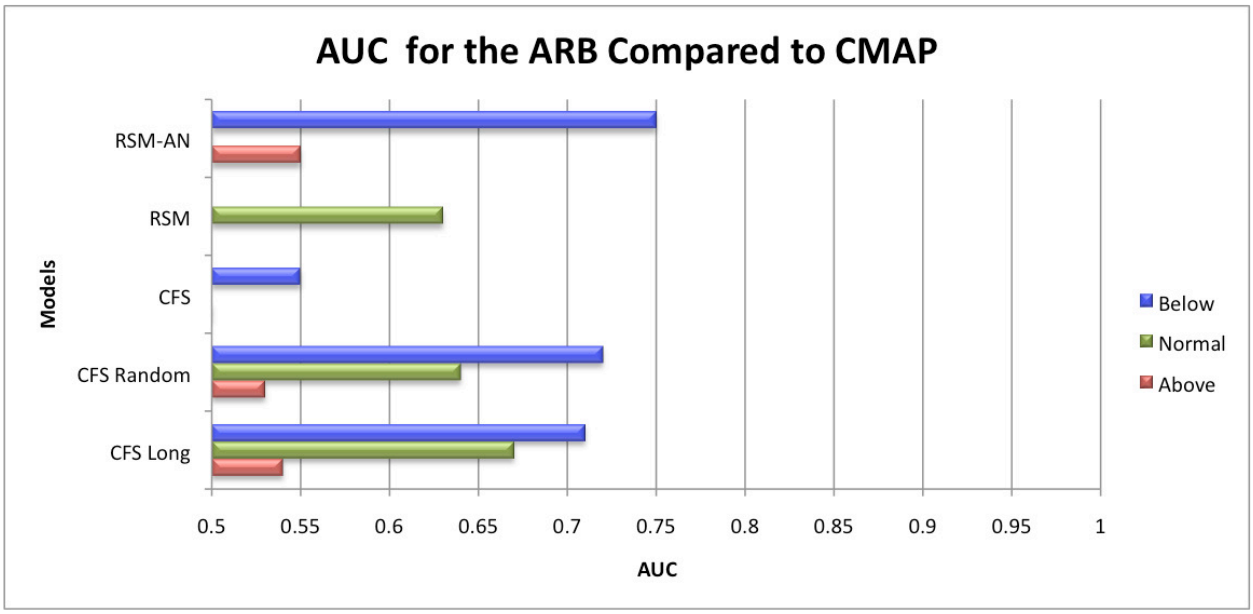

Figure 3.14 Same as Figure 3.12 except using CMAP as a comparison dataset and the CFS integration with 15 ensemble members and a randomly chosen 7 years is no longer displayed.

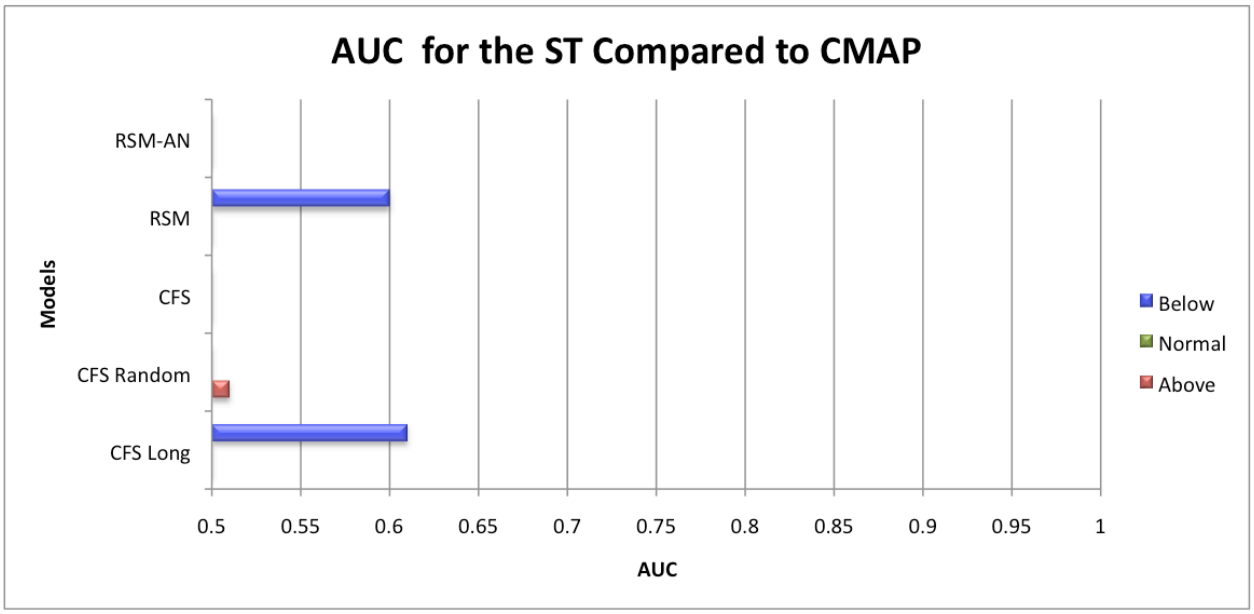

Figure 3.15 Same as Figure 3.14 except the region has changed to the ST.

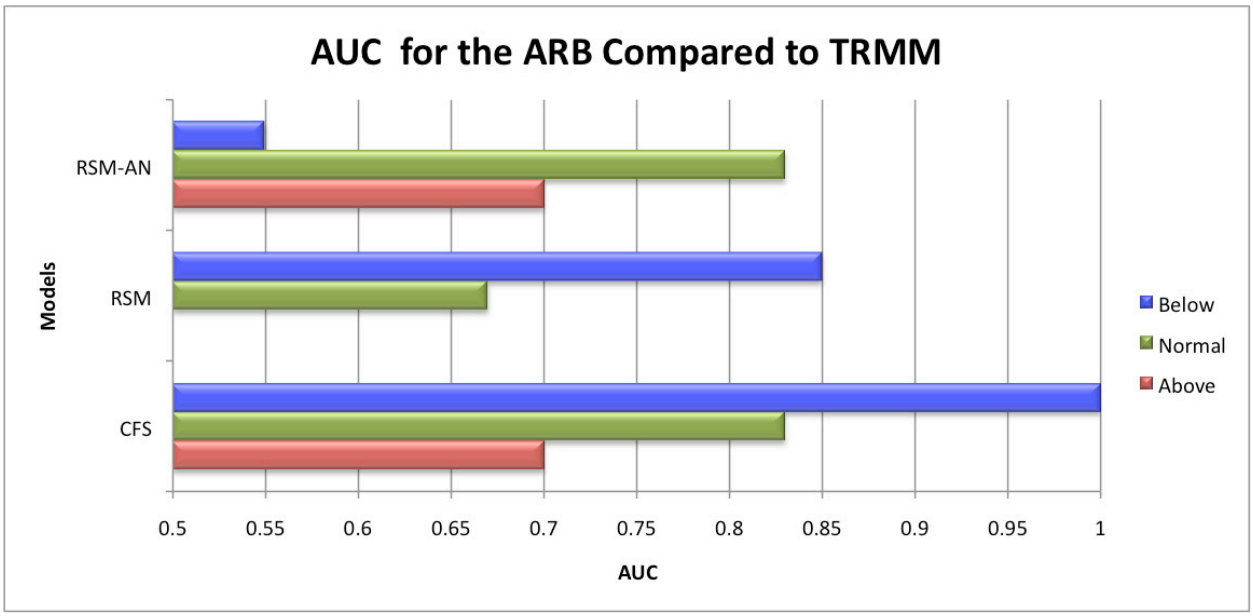

Figure 3.16 Same as Figure 3.14 except TRMM is now the comparison dataset and none of the supplementary CFS integrations are included (i.e., only the three primary model runs are shown).

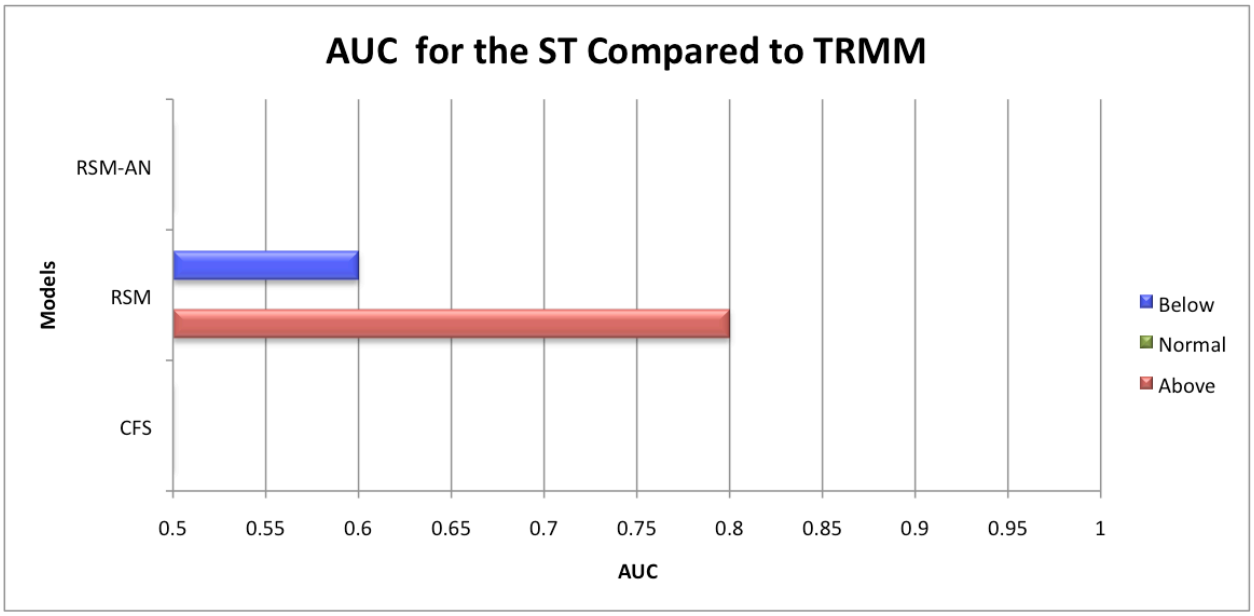

Figure 3.17 Same as Figure 3.16 except the region has now changed to the ST.

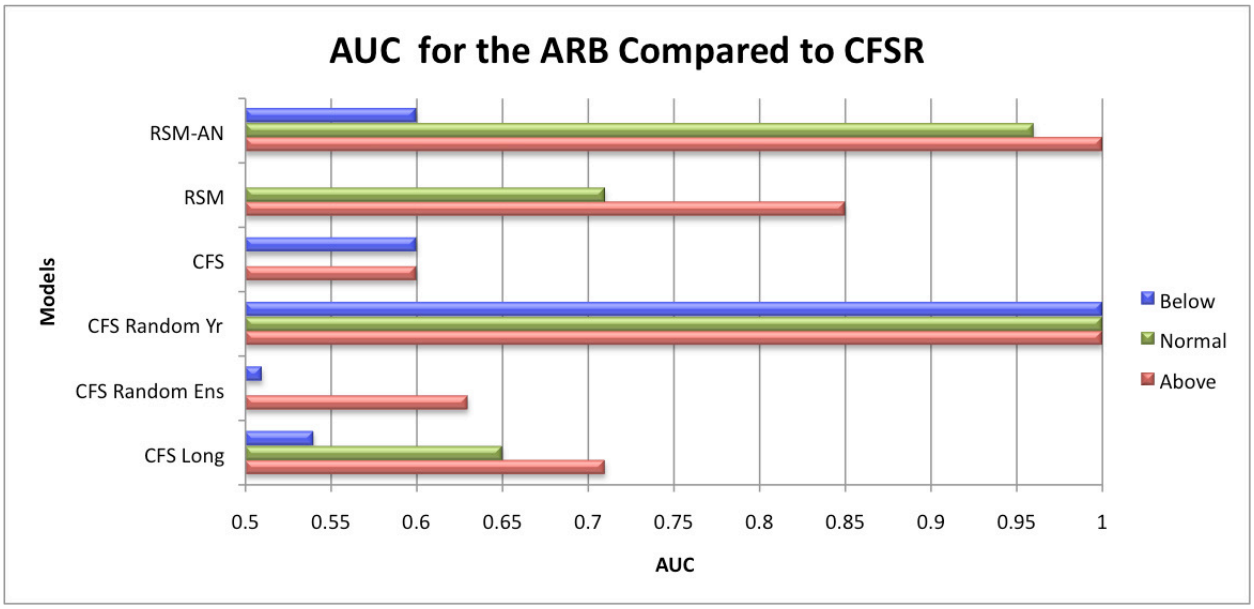

Figure 3.18 Same as Figure 3.12 except the variable is two-meter air temperature.

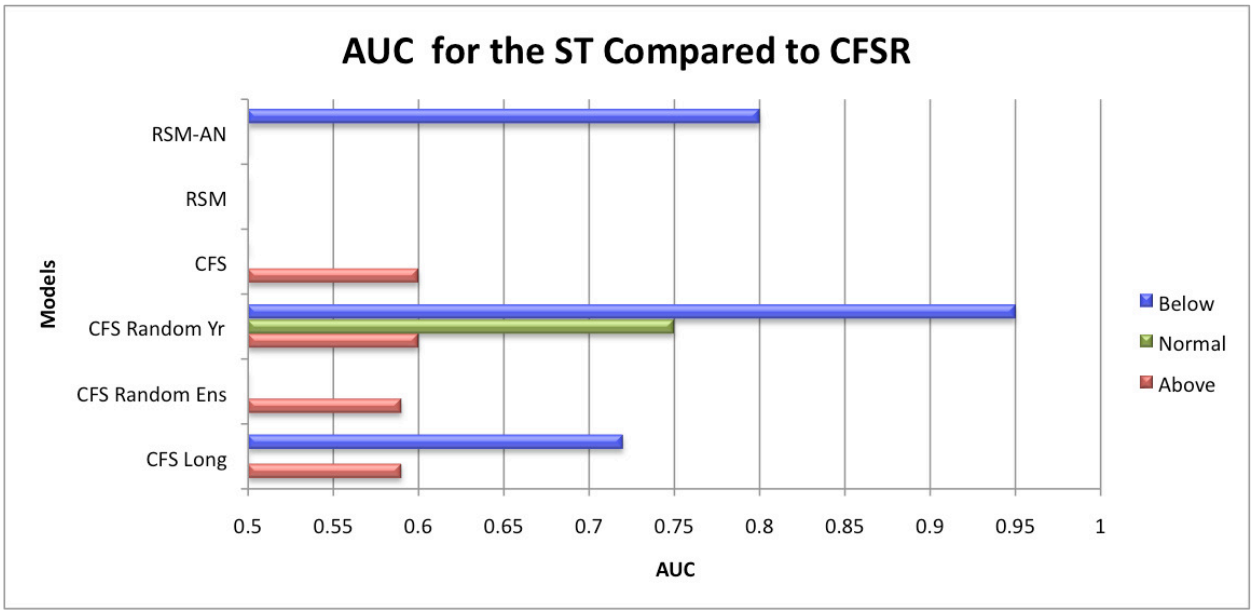

Figure 3.19 Same as Figure 3.18 except the region has changed to the ST.

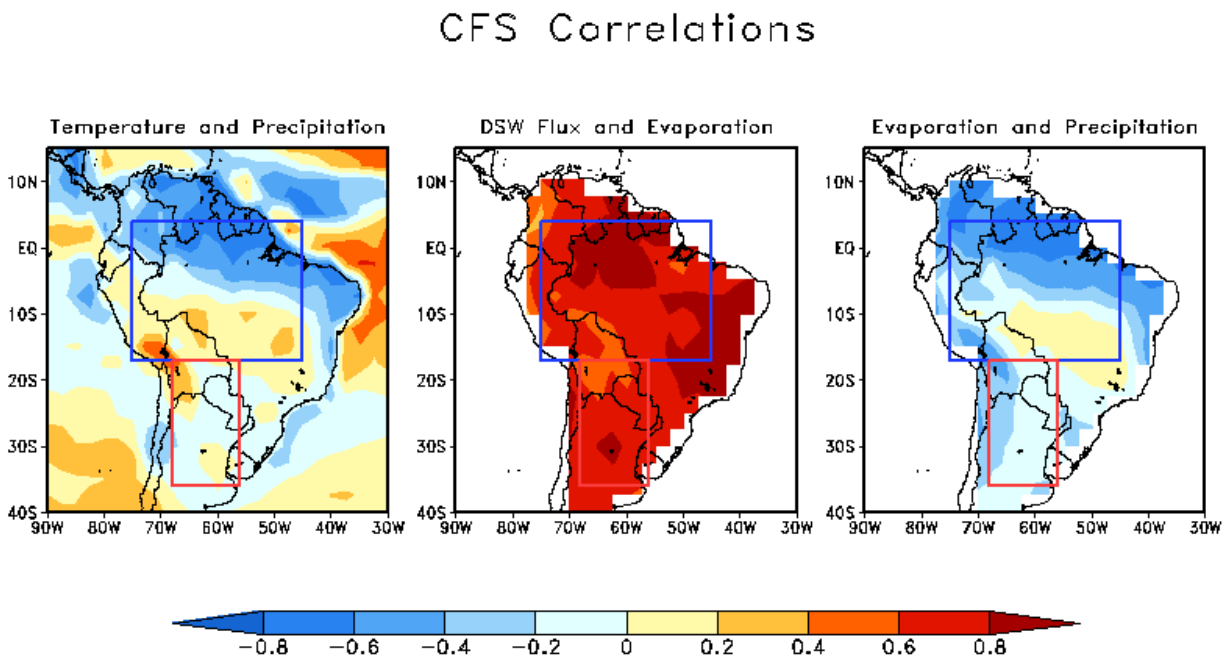

Figure 3.20 Contemporaneous correlations between temperature and precipitation (left), downwelling shortwave flux and evaporation (middle), and evaporation and precipitation (right) in the CFS model. Correlations are calculated using the model six-hourly data from JJA for the years 2001–2007.

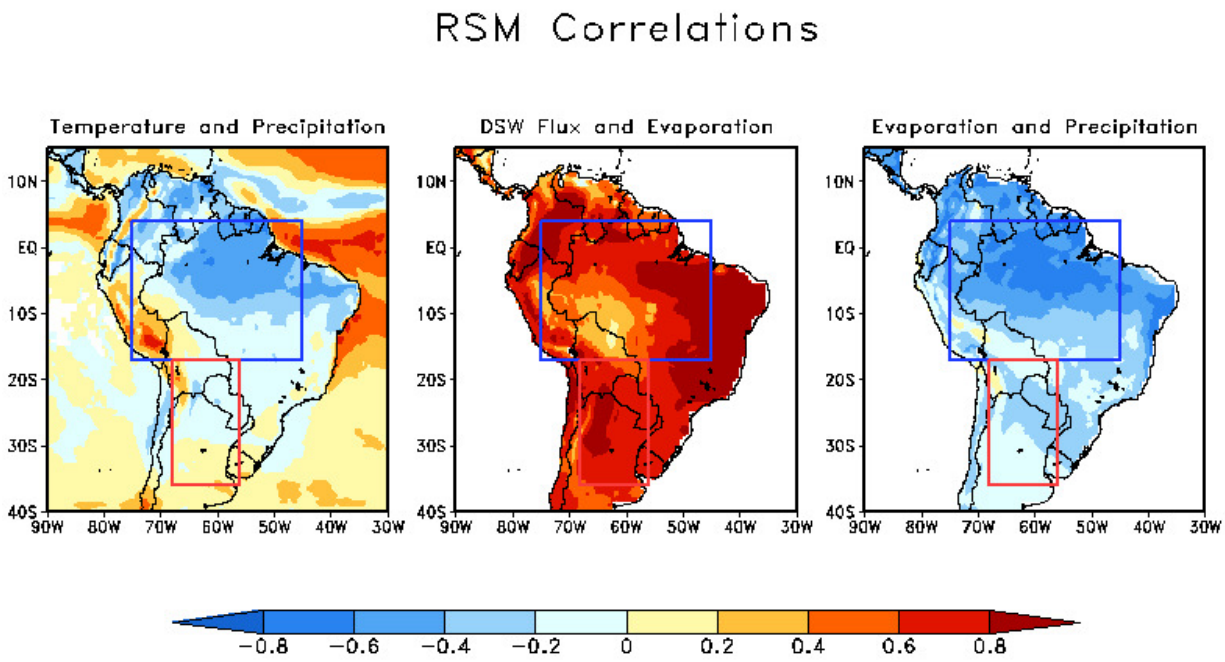

Figure 3.21 Same as Figure 3.20 except the model is the RSM.

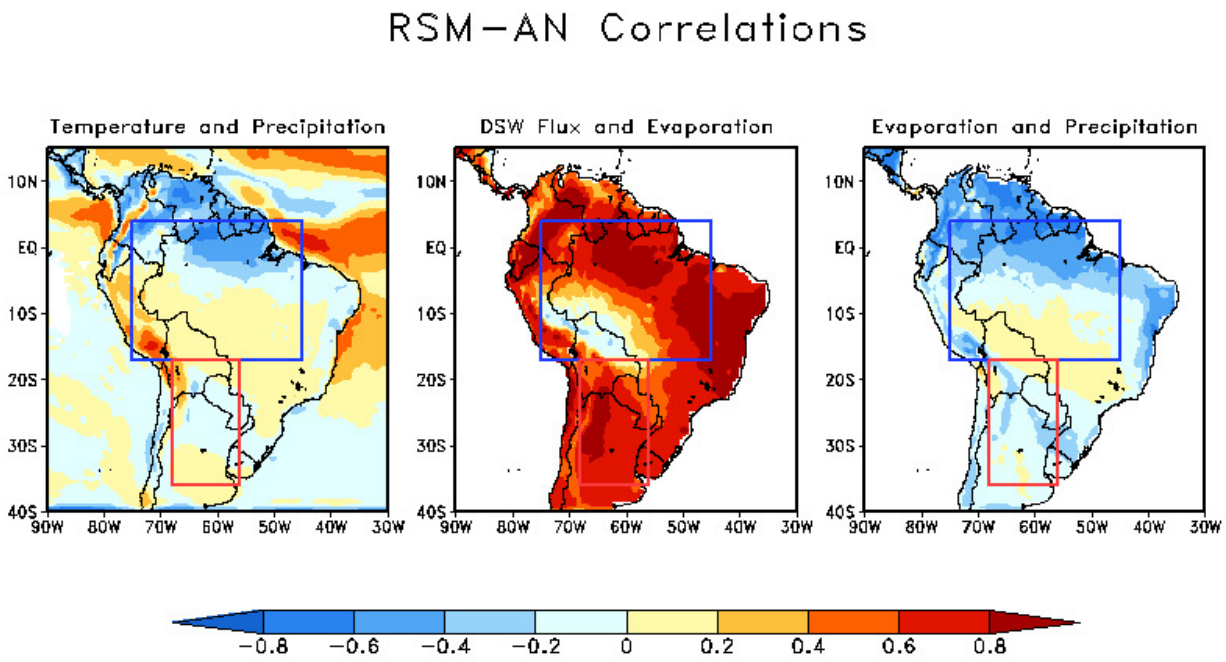

Figure 3.22 Same as Figure 3.20 except the model is the RSM-AN.

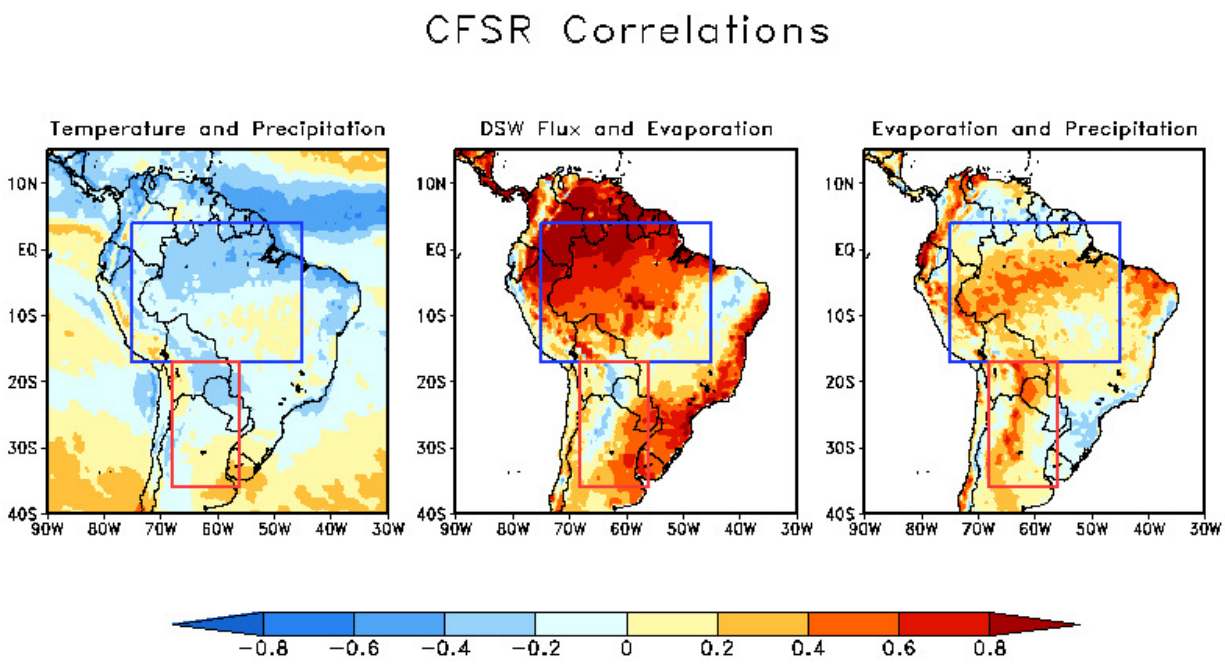

Figure 3.23 Same as Figure 3.20 except for CFSR is now being shown.

CHAPTER FOUR

CONCLUSIONS

In this study, we analyzed the output of three climate model integrations, the NCEP CFS, the NCEP Scripps RSM with unmodified CFS data, and the NCEP Scripps RSM with bias correction applied to the CFS data, for seven dry seasons of the South American monsoon. The three primary objectives of this research were to analyze the biases of precipitation and of two-meter air temperature in the models, to investigate the models' skill in predicting those two variables, and to identify a possible reason for the model solutions differing from the reanalysis data by undertaking an investigation of land-atmosphere feedbacks within the models and the reanalysis. In this study, we focused on two primary regions: the Amazon River Basin and the subtropical region.

The primary comparison dataset used in this study was NCEP CFSR. However, since some CFSR variables are produced using a model, we also compared CFSR to other, more widely used datasets. For example, CFSR two-meter air temperature was compared with CRU two-meter air temperature. We found that most areas exhibited five-year (2001-2005) dry season average differences of less than 1-2°C. The exception to this was over elevated terrain, where differences occasionally exceeded 3°C. As a result, CFSR was considered a reasonable representation of two-meter air temperature over SA. Additionally, CFSR precipitation was compared to CMAP and TRMM precipitation. CFSR was negatively biased in the ARB and positively biased in the ST, although biases were generally low. As a result, CFSR was also considered a reasonable representation of precipitation during the dry season.

We found that all three models, when compared to CFSR, exhibited positive biases of two-meter air temperature in the ARB, where the CFS possessed the largest bias. In the ST, the CFS was negatively biased, whereas the RSM and the RSM-AN were positively biased. When we compared the models' precipitation to CFSR's precipitation we found that the CFS and the RSM-AN were both negatively biased in each region and that the RSM was positively biased in each region. The differences between precipitation in CFSR and TRMM and between precipitation in CFSR and CMAP were small enough that we did not expect any drastic differences between our comparison of the models with CFSR or with those two datasets. When

we analyzed the results from all three comparisons (i.e., models compared to CFSR, TRMM, and CMAP) we found that although the sign of the bias for a particular model and region did not always remain the same, the magnitude of the bias usually did.

Differences were found between potential predictability ratios in the ARB and in the ST. For both precipitation and two-meter air temperature and for all models, the ARB exhibited larger ratios than did the ST, which indicated that the models more easily "saw" the boundary conditions in the ARB. The potential predictability ratios also indicated that the models better differentiated between different temperature regimes than between different precipitation regimes, particularly in the ARB. Potential predictability ratios are not necessarily indicative of a model's skill. However, in this study, where the differences between ratios from different regions or from different variables are large (no specific value has been defined), the potential predictability was a fair first-approximation of model skill.

ROC curve analysis for precipitation using CFSR as a comparison dataset indicated that applying the downscaling and anomaly nesting processes yielded the most skill in the ARB, whereas applying only downscaling yielded the most skill in the ST. When analyzing two-meter air temperature, we found it most beneficial to apply the downscaling and anomaly nesting processes in both regions. The same conclusions were reached using CMAP as a comparison dataset. Interestingly, when using TRMM as our comparison dataset, we found no added benefit to applying either the downscaling or the anomaly nesting methods in the ARB, but our conclusions for the ST were identical to those reached when we used CFSR and CMAP.

The difference between the results achieved by using different datasets is evidence of one limitation of this study. We used only seven years and six ensemble members in our model integrations. As a result, small differences between comparison datasets (i.e., CFSR, TRMM, and CMAP) can have large impacts on the results of our ROC curve analysis. However, CFSR's and CMAP's providing identical conclusions, and TRMM's providing similar conclusions, suggests that we have acquired an adequate representation of the models' skill. It is promising that the primary differences we observed between different observational datasets were between the specific scores achieved by different models in different regions, and not with our larger scale conclusions. Additionally, using a longer integration of the CFS (23 years), with more ensemble members, we determined that reducing the number of ensemble members did not largely change the results of the ROC analysis. However, when we reduced the number of years

in the longer CFS integration from 23 to 7, some differences arose in the results of the ROC curve analysis. In the future, if it becomes computationally feasible, we would like to add more years to all three model integrations (CFS, RSM, and RSM-AN) and repeat the process.

The investigation into land-atmosphere interactions within the models and within CFSR provided a possible reason for the models exhibiting less-than-perfect skill in our ROC curve analysis. According to Koster et al. (2003) in the models, correlations of temperature and precipitation indicated that evaporation was leading to precipitation. However, negative correlations of precipitation with evaporation indicated that evaporation was not leading to precipitation over much of SA. Additionally, mostly positive correlations of evaporation and downwelling flux suggested that evaporation was energy limited in the models. Therefore, the models have indicated that, during the dry season, SA has an arid climate in which evaporation is energy limited and is not sufficient to fuel precipitation. This implies that additional moisture must be advected from remote locations. CFSR exhibited mostly positive correlations between evaporation and precipitation, which suggested that local evaporation, rather than remote advection of moisture, contributed most significantly to precipitation over SA. The difference between the models and CFSR is potentially a consequence of the models producing less precipitation than CFSR and thus being more arid than CFSR.

Our results have indicated that downscaling and anomaly nesting could be beneficial to forecasts for the South American dry season. However, we must remember that the ROC scores are also dependent on the dataset that we choose to compare the models to, as well as the years that we choose to analyze. We have suggested that incorrect land-atmosphere feedbacks in the models could account for differences between the models and CFSR which could, in turn, lead to imperfect ROC scores. To completely resolve land-atmosphere feedbacks in the models and in CFSR, a full moisture budget analysis is needed. Unfortunately, a full moisture budget is beyond the scope of this research. A similar modeling study including more, or different, years and more ensemble members is recommended.

APPENDIX A

RANKING OF THE YEARS IN PRIMAR Y DATASET

Table A.1 Shows the years ranked from highest to lowest for two-meter air temperatures in the ST for our different datasets. The years correspond to values that are calculated by finding the JJA average for all grid points and then area averaging over all grid points in the ST. For the models the ensemble mean is used.

2m T in ST	CMAP	TRMM	CFSR	CFS	RSM	RSM-AN
1. Wettest	2005	2005	2005	2003	2002	2002
2	2006	2001	2004	2002	2001	2001
3	2002	2002	2006	2001	2005	2007
4	2004	2004	2002	2004	2007	2006
5	2001	2006	2003	2005	2003	2003
6	2003	2003	2001	2007	2006	2005
7. Driest	2007	2007	2007	2006	2004	2004

Table A.2 Same as Table A-1 except for ARB.

2m T in ARB	CMAP	TRMM	CFSR	CFS	RSM	RSM-AN
1. Wettest	2006	2003	2007	2001	2001	2003
2	2007	2004	2003	2003	2006	2007
3	2004	2002	2006	2002	2002	2001
4	2003	2006	2004	2006	2003	2006
5	2002	2001	2001	2004	2007	2005
6	2005	2007	2005	2007	2005	2002
7. Driest	2001	2005	2002	2005	2004	2004

Table A.3 Same as Table A-1 except for precipitation rate.

Precip in ST	CFSR	CFS	RSM	RSM-AN
1. Warmest	2006	2001	2005	2005
2	2001	2007	2004	2004
3	2005	2005	2007	2001
4	2004	2004	2001	2006
5	2003	2002	2006	2002
6	2002	2006	2003	2007
7. Coldest	2007	2003	2002	2003

Table A.4 Same as Table A-3 except for the ARB.

Precip in ARB	CFSR	CFS	RSM	RSM-AN
1. Warmest	2002	2005	2005	2005
2	2005	2004	2004	2004
3	2006	2002	2002	2002
4	2001	2007	2007	2001
5	2007	2006	2003	2007
6	2003	2001	2001	2006
7. Coldest	2004	2003	2006	2003

REFERENCES

Behringer, D. W., and Y. Xue, 2004: Evaluation of the global ocean data assimilation system at NCEP: The Pacific Ocean. 8th symposium on integrated and observation system for atmosphere, ocean and land surface. AMS 84th annual meeting, Washington State Convention15 and Trade Center, Seattle, Washington 11-15.

Chan, S.C. and V. Misra, 2009: Dynamic Downscaling of the North American Monsoon with the NCEP Scripps Regional Spectral Model from the NCEP CFS global model. Submitted to *J. Climate*

Druyan, L. M., M. Fulakeza, and L. Patric, 2002: Dynamic downscaling of seasonal climate predictions over Brazil. *J. Climate,* **15,** 84–117.

Ek, M. B., and Coauthors, 2003: Implementation of the upgraded Noah land-surface model in the NCEP operational mesoscale Eta model. *J. Geophys. Res.,* **108,** 8851, doi:10.1029/2002JD003296.

Fasullo, J., and P. J. Webster, 2003: A hydrological definition of Indian monsoon onset and withdrawal. *J. Climate,* **16,** 3200–3211.

Hong, S. Y., and H. L. Pan, 1996: Nonlocal boundary layer vertical diffusion in a medium-range forecast model. *Mon. Wea. Rev.,* **124,** 2322-2339.

_____ and _____, 1998: Convective trigger function for a mass-flux cumulus parameterization scheme. *Mon. Wea. Rev.,* **126,** 2599- 2620.

Juang, H. M., and M. Kanamitsu, 1994: The NMC nested regional spectral model. *Mon. Wea. Rev.,* **122,** 3-26.

Koster, R. D., and Coauthors, 2003: Observational evidence that soil moisture variations affect precipitation. *Geophys. Res. Lett*., **30**, 1241, doi:10.1029/2002GL016571.

Liebmann, B., and Coauthors, 2004: Subseasonal variations of rainfall in South America in the vicinity of the low-level jet east of the Andes and comparison to those in the South Atlantic convergence zone. *J. Climate,* **17,** 3829–3842.

Kanamaru, H., and M. Kanamitsu, 2007: Scale-selective bias correction in a downscaling of global analysis using a regional model. *Mon. Wea. Rev.,* **135,** 334-350.

Kanamitsu, M., and Coauthors, 2002: NCEP-DOE AMIP-II Reanalysis (R-2). *Bull. Amer. Meteor. Soc.,* **83,** 1631-1643.

Kumar, A., and M.P. Hoerling, 1995: Prospects and limitations of seasonal atmospheric GCM predictions. *Bull. Amer. Meteor. Soc.,* **76**, 335-345.

Mahrt, L., and H.-L. Pan, 1987: 1 A two-layer model of soil hydrology. *Bound.-Layer Meteor.,* **29,** 1-20.

Mason, S. J., and N. E. Graham, 1999: Conditional probabilities, relative operating characteristics and relative operating levels. *Wea. Forecasting,* **14,** 713–725.

Misra, V., and P. A. Dirmeyer, 2009: Air, Sea, and Land Interactions of the Continental US Hydroclimate. *J. Hydromet*., **10**, 353-373.

Misra, V. and M. Kanamitsu, 2004: Anomaly nesting: a methodology to downscale seasonal 8 climate simulations from AGCMs. *J. Climate,* **17**, 3249-3262.

Myneni, R. B., et al., 2007: Large seasonal swings in leaf area of Amazon rainforests. *Proc Natl Acad. Sci. USA. 104, 4820-4823*

Noguer, M., R. G. Jones, and J. Murphy, 1998: Sources of systematic errors in the climatology of a nested regional climate model (RCM) over Europe. *Climate Dyn.,* **14,** 691–712.

Pan, Z., and Coauthors, 2001: Evaluation of uncertainties in regional climate change simulations. *J. Geophys. Res.,* **106,** 17 735–17 752.

Raia, A, Cavalcanti IFA, 2008: The life cycle of the South American monsoon system. *Journal of Climate* **21**: 6227–6246.

Roads, J. O., and S-C. Chen, 2000: Surface water and energy budgets in the NCEP regional spectral model. *J. Geophys. Res.,* **105,** 29 539–29 550.

——, ——, and M. Kanamitsu, 2003: U.S. regional climate simulations and seasonal forecasts. *J. Geophys. Res.,* **108,** 8606, doi:10.1029/2002JO002232.

Saha, S., and Coauthors, 2006: The NCEP Climate Forecast System.*J. Climate,* **19,** 3483–3517.

Saha, S., et al., 2010: The NCEP Climate Forecast Reanalysis. Bull. Amer. Meteor. Soc., **91**, 1015-1057.

Stefanova, L., and Coauthors, 2010: Hindcast skill and predictability for precipitation and two-meter air temperature anomalies in global circulation models over the Southeast United States. *Climate Dyn.,*

Vera, C., and Coauthors, 2006: Toward a unified view of the American monsoon systems. *J Climate* **19**:4977–5000

Wang, C., S.-K. Lee, and D.B. Enfield, 2008: Climate response to anomalously large and small Atlantic warm pools during the summer. *Journal of Climate* **21**: 2437–2450.

Xie, P., and P.A. Arkin, 1997: Global precipitation: A 17-year monthly analysis based on gauge observations, satellite estimates, and numerical model outputs. *Bull. Amer. Meteor. Soc*., **78**, 2539 - 2558.

Zhou, J., and K.-M. Lau, 1998: Does a monsoon climate exist over South America? *J. Climate*, **11**, 1020–1040.

BIOGRAPHICAL SKETCH

Adam Frumkin was born in Nashua, NH on January 8th 1987. He became interested in meteorology at a very young age. In 2004 while on vacation in Orlando, FL he experienced the devastation of hurricane Charley, and made an impromptu visit to the Florida Institute of Technology's Meteorology Department. It was at that time that he made the decision to pursue a career in meteorology. Unable to afford a move to Florida, he opted to study Meteorology at Plymouth State University in Plymouth, NH where he graduated summa cum laude with a Bachelor's degree in Meteorology in 2009. Excited to continue his education and eager to avoid a recession ravaged job market he opted to attend graduate school at The Florida State University. While at FSU he has studied under the guidance of Dr. Vasu Misra and his research has focused on climate modeling and forecast verification. Although his career goals have changed since entering FSU, he hopes to be able to incorporate the skills he has acquired here in his future endeavors. In his spare time he enjoys photography, hiking, and automotive technology.